

Mantle Dynamics in Mars and Venus: Influence of an Immobile Lithosphere on Three-Dimensional Mantle Convection

G. SCHUBERT AND D. BERCOVICI¹

Department of Earth and Space Sciences, University of California, Los Angeles

G. A. GLATZMAIER

Earth and Space Sciences Division, Los Alamos National Laboratory, Los Alamos, New Mexico

Numerical calculations of fully three-dimensional convection in constant viscosity, compressible spherical shells are interpreted in terms of possible convective motions in the mantles of Venus and Mars. The shells are heated both internally and from below to account for radiogenic heating, secular cooling, and heat flow from the core. The lower boundary of each of the shells is isothermal and shear stress free, as appropriate to the interface between a mantle and a liquid outer core. The upper boundary of each of the shells is rigid and isothermal, as appropriate to the base of a thick immobile lithosphere. Calculations with shear stress-free upper boundaries are also carried out to assess the role of the rigid surface condition. The ratio of the inner radius of each shell to its outer radius is in accordance with possible core sizes in both Venus and Mars. A calculation is also carried out for a Mars model with a small core to simulate mantle convection during early core formation. Different relative proportions of internal and bottom heating are investigated, ranging from nearly complete heating from within to almost all heating from below. The Rayleigh numbers of all the cases are approximately 100 times the critical Rayleigh numbers for the onset of convection. Cylindrical plumes are the prominent form of upwelling in the models independent of the surface boundary condition so long as sufficient heat derives from the core. Thus major volcanic centers on Mars, such as Tharsis and Elysium, and the coronae and some equatorial highlands on Venus may be the surface expressions of cylindrical mantle plumes. The form of the downwelling sheets is significantly affected by the rigid boundary in that the sheets are more irregular in their horizontal structure than when the top boundary is shear stress free. In the mainly heated-from-within models, the downwelling sheets are also shorter and less temporally durable when the top boundary is rigid than when it is stress free. Thus the free motion of plates on the Earth facilitates extensive durable convective currents that drive the plates, while the stiffening of the lithospheres on Mars and Venus promotes a style of convection that is not particularly effective in breaking the lithosphere into plates. In the rigid top cases, the upper boundary layer surrounding the plumes appears to be interspersed with downwelling currents emanating radially from the plumes' axes; these currents may establish a stress field at the base of hotspot swells that could lead to radial fractures such as those on Tharsis. Models with rigid upper boundaries have higher interior temperatures than do similar models with shear-stress-free upper boundaries. On this basis, Venus not only has a higher surface temperature than Earth, but it would have a hotter mantle as well. Upwelling plumes are more numerous when the outer boundary is rigid (as compared with shear stress free). Flows dominated by a few strong plumes occur when the proportion of basal heating is large. Thus if the Martian crustal dichotomy were caused by a convective system dominated by spherical harmonic degree $\ell = 1$, then the convection may have been driven strongly from below by a heating pulse accompanying core formation or from the flow of heat from an early hot core. If a convective mechanism is responsible for the crustal dichotomy, then the dichotomy is likely a very ancient feature. However, the small core models we consider consistently produce a convective pattern with a dominant $\ell = 2$ signature which does not correlate with the Martian crustal dichotomy; a yet smaller core may be necessary to yield the $\ell = 1$ pattern. The small core convective pattern does correlate with the geoid and topography signatures of Tharsis, which have strong $\ell = 2$ components, and the model produces dynamic uplift comparable to the total topography of the Tharsis rise. Models with larger cores (i.e., with the probable inner to outer radius ratio of Mars' present mantle) generate 4 km of uncompensated topography, similar to estimates of the uncompensated Tharsis topography. Thus the Tharsis rise could have achieved its full height early in the evolution of Mars by mantle plume dynamic uplift. At present, the uncompensated portion of the Tharsis rise topography can be accounted for by dynamic uplift, obviating the need for elastic support. The present compensated portion of the Tharsis topography could be attributed to volcanic or magmatic crustal thickening or depletion of the underlying mantle. Large core models appropriate to the present Mars produce too many plumes to account for just two major volcanic centers (i.e., Tharsis and Elysium). Mantle plume activity could be focussed beneath regions like Tharsis if fracturing or thinning of the lithosphere in these regions has facilitated magma and heat transport across the lithosphere. A similar mechanism could be responsible for clustering of coronae on Venus. There are no deep-seated, active, linear upwellings in the Venus models that could be associated with linear spreading centers in Aphrodite. If linear spreading is actually occurring in Aphrodite, the phenomenon is probably a shallow passive one, similar to mid-ocean ridges on Earth.

Copyright 1990 by the American Geophysical Union.

¹ Now at the Department of Geology and Geophysics, Woods Hole Oceanographic Institution, Woods Hole, Massachusetts.

Paper number 90JB00836.
0148-0227/90/90JB-00836\$05.00

INTRODUCTION

It is generally agreed that subsolidus mantle convection is the means by which the terrestrial planets transfer heat from their deep interiors to the surface [e.g., Schubert, 1979]. Yet, until recently, the difficulty of modelling fully three-dimensional compressible convection in spherical geometry has precluded the possibility of deducing the style of these convective motions. With the advent of supercomputers, that situation has changed, allowing for the development of numerical models of large-scale mantle convection [Glatzmaier, 1988; Baumgardner, 1988]. One model [Glatzmaier, 1988] has been validated and applied to convection in the Earth's mantle [Bercovici et al., 1989a,b,c]. Model results indicate that mantle convection in the Earth is characterized by cylindrical upwelling plumes surrounded by descending planar sheets and that there are no active sheetlike upwellings [Bercovici et al., 1989b,c]. The linear ridge system on Earth represents a shallow, passive upwelling due to the tearing of the plates by the pull of descending slabs. More realistic models of Earth with plate-like rheological behavior are required to reproduce this characteristic of plate tectonics.

Venus and Mars differ from Earth in fundamental ways that might cause convection in these planets to differ from mantle convection in the Earth. From the viewpoint of differences that the numerical model is capable of addressing, the most important is the absence of plate tectonics on Venus [Kaula and Phillips, 1981; Phillips et al., 1981] and Mars. Venus and Mars are one-plate planets [Solomon, 1978; Schubert et al., 1979] with rigid, immobile lithospheres. Mantle convection in Venus and Mars thus occurs beneath a rigid lid, making the vanishing of the velocity at the outer surface of the model spherical shell the appropriate mechanical boundary condition for numerical simulations. The mobile tectonic plates on Earth are an integral part of the mantle convection system, making free slip or the vanishing of the shear-stress the appropriate mechanical boundary condition at the outer surface of the model shell. Other differences between Mars on the one hand and Earth and Venus on the other include the relatively small compression of the Martian mantle due to its smaller size and gravity. There are, of course, still additional differences among the terrestrial planets, both known and unknown, that may be important in altering the styles of mantle convection in these planets. However, we deal only with the differences, identified above, that can be readily accounted for in the numerical model.

The objectives of this paper, accordingly, are to investigate the style of mantle convection in planets with rigid lids such as Venus and Mars and, by comparison with results for convection with shear stress-free upper surfaces, to delineate the effects of the rigid upper boundary condition. We begin with a brief description of the model, the equations, the boundary conditions, and the numerical method. We then discuss the results of the numerical calculations and their implications for Venus and Mars.

MODEL, NUMERICAL APPROACH,
AND PARAMETER VALUES

In this section we only briefly describe the model and refer the reader to Glatzmaier [1988] and Bercovici et al. [1989a] for a detailed description. The model consists of a spherical

shell of compressible fluid with constant viscosity μ and thermal conductivity k . The acceleration of gravity \bar{g} is radially inward and is due to a central gravity field of a homogeneous core and the self-gravitation of the mantle; \bar{g} therefore varies with radius r and is self-consistently determined together with the mantle density distribution $\bar{\rho}(r)$ in the hydrostatic, adiabatic, reference state. The density $\bar{\rho}$ and pressure \bar{p} in the basic state are related by the Murnaghan equation for the adiabatic bulk modulus \bar{K} ,

$$\bar{\rho} \frac{d\bar{p}}{d\bar{p}} = \bar{K}_s = K_o + K' \bar{p} \quad (1)$$

where K_o and K' are constants.

The dynamic state is represented by the perturbations in pressure p' , entropy s' , density ρ' , and temperature T' . The convective state is governed by the anelastic equations of mass, momentum and energy conservation

$$\nabla \cdot (\bar{\rho} \underline{v}') = 0 \quad (2)$$

$$-\nabla p' + \mu \nabla^2 \underline{v}' + \frac{\mu}{3} \nabla (\nabla \cdot \underline{v}') - \rho' \bar{g} \hat{x} = 0 \quad (3)$$

$$\bar{\rho} \bar{T} \left(\frac{\partial s'}{\partial t} + \underline{v}' \cdot \nabla s' \right) = k \nabla^2 (\bar{T} + T') + \underline{\underline{\sigma}} : \underline{\underline{\epsilon}} + Q \quad (4)$$

where \underline{v}' is the convective velocity, \hat{x} is the unit vector in the radial direction, $\bar{T}(r)$ is the temperature in the adiabatic reference state, $\underline{\underline{\epsilon}}$ is the rate of strain tensor, $\underline{\underline{\sigma}}$ is the deviatoric stress tensor, and Q is the rate of internal energy generation per unit volume (the rate of internal energy generation per unit mass $\epsilon \equiv Q/\bar{\rho}$ is assumed constant). The energy equation accounts for heating due to viscous dissipation, as is necessary in compressible convection. The momentum equation neglects inertial forces as is appropriate to the highly viscous mantles of the terrestrial planets. The solenoidal mass flux $\bar{\rho} \underline{v}'$ can be expressed in terms of poloidal and toroidal functions [Chandrasekhar, 1961; Glatzmaier, 1984, 1988], and it is consistent with the spherically symmetric viscosity and homogeneous (i.e., nonforced) boundary conditions to take the toroidal part equal to zero.

We apply shear-stress-free, impermeable, and isothermal boundary conditions at the inner radius of the spherical shell as appropriate to the interface between a mantle and a liquid outer core. Although, the inferred lack of magnetic fields on Mars and Venus imply either a completely solid or completely molten core, liquid core models are consistent with thermal histories [Stevenson et al., 1983; Schubert and Spohn, this issue]. Moreover, test simulations with a solid core did not produce significant differences from the simulations with the molten core. Thus it is tacitly assumed that Venus and Mars have cores that are still liquid at least in their outer parts. The outer radius of the shell is considered to be the base of the rigid lithosphere. The bottom of the lithosphere is a rheological boundary determined by the viscosity at which mantle rocks can readily flow on a geologic time scale. Since rock viscosity is mainly determined by temperature, one may assume that the base of the lithosphere occurs along a constant value of the homologous temperature. Deflections of this boundary are upward if a hot temperature anomaly impinges on it (and downward for a cold temperature anomaly); thus the deflection

essentially restores the boundary to its homologous temperature by moving it up (or down) the geotherm. If the deflection to lower (or higher) pressures is not great enough to cause a significant change in the melting temperature, then a boundary of constant homologous temperature can be approximated by an isotherm. Thus the base of the lithosphere is assumed to be isothermal, and we apply a constant temperature boundary condition to the outer surface of the mantle shell. This surface is also assumed to be an impermeable rigid boundary so that all velocity components vanish at the boundary, as appropriate to flow beneath an immobile lid. Application of a rigid, isothermal boundary condition at the outer radius of the model shell ignores lithosphere thickness variations. However, such thickness variations are not expected to have a zeroth order effect on the basic pattern of convection. Solely for the purpose of evaluating the effects of the rigid boundary condition, we also carry out calculations with the outer surface of the shell taken to be an impermeable, shear-stress-free boundary.

The numerical approach is based on a pseudospectral, Chebyshev collocation scheme in which spherical harmonics are used to represent latitudinal and longitudinal variability in the solutions and Chebyshev functions are used to represent radial variability [Glatzmaier, 1984, 1988]. The numerical results are obtained using 96 longitudinal grid points, 48 latitudinal points for those cases with a large component of basal heating; 128 longitudinal and 64 latitudinal points are used for cases with a large component of internal heating. The different resolutions are used because internal heating leads to small-wavelength features and the largest lateral thermal gradients occur near the top boundary (because the temperature drop and thus the thermal anomalies are greatest in the upper boundary layer) where horizontal resolution is poorest. All cases have 41 radial grid points. Latitudinal, longitudinal and radial grid spacings are given in Tables 1, 2, and 4. It is evident from these tables that Chebyshev collocation points are naturally weighted toward the boundaries, and thus provide higher radial resolution of the top and bottom boundary layers. The accuracy of the solutions can be estimated from the power spectra of the dependent variables in spectral wave number space (Figure 1). A drop in spectral power of 3-4 orders of magnitude from the leading mode to the mode near truncation indicates that the solutions are reasonably well resolved. The velocity field is better resolved than the entropy field. The entropy field is only marginally resolved, especially near the outer boundary of the largely internally heated models. Additional calculations at twice the horizontal resolution, not shown here, indicate that while even more horizontal resolution is required for the fine structure of the entropy field, the large-scale thermal structures are properly represented even at the resolution of this paper. Time stepping is done using an explicit Adams-Bashforth scheme for the nonlinear terms and an implicit Crank-Nicolson scheme for the linear terms. The exact time steps are constrained by the Courant condition. Each set of results discussed later involves integration over about 10^4 time steps. Thus the simulations were integrated through on the order of ten convective overturn times after the solutions became statistically steady.

The input and output parameter values for each of the solutions presented here are listed in Tables 1-4. Although the compressible solutions are characterized by nine nondimensional parameters and the Boussinesq solutions by four

TABLE 1. Input Parameters for Mars and Venus Models

Parameter	Value
<i>Mars</i>	
r_{top} , km	3200
r_{bot} , km	1762
$\bar{\rho}$, kg/m ³	3450
\bar{T} , K	1500
M_{core} , kg	1.49×10^{23}
$\bar{\alpha}$, K ⁻¹	2×10^{-5}
ΔT_{sa} , K	800
k , W/K/m	4.14
c_p , kJ/K/kg	12
Δr_{mid}^* , km	56
Δr_{top}^* , Δr_{bot}^* , km	2
N^{**}	20
<i>Venus</i>	
r_{top} , km	6051.5
r_{bot} , km	3110
$\bar{\rho}_{top}$, kg/m ³	3300
$\bar{\rho}_{bot}$, kg/m ³	5450
\bar{T}_{bot} , K	2000
γ^\dagger	1
K'	3.5
K_0 , Pa	9.25×10^{10}
M_{core} , kg	1.575×10^{24}
ΔT_{sa} , K	2000
k , W/K/m	6.54
c_p , kJ/K/kg	12
Δr_{mid}^* , km	116
Δr_{top}^* , Δr_{bot}^* , km	5
N^{**}	20

* Δr_{mid} is the radial grid spacing midway through the shell; Δr_{top} and Δr_{bot} are the radial grid spacings near the top and bottom boundaries of the shell.

** N is the truncation level of the Chebyshev series (i.e., the maximum Chebyshev degree is N).

† $\gamma = d(\ln \bar{T})/d(\ln \bar{\rho})$ is the Grüneisen parameter.

[see Bercovici *et al.*, 1989b,c], the important parameters are the Rayleigh numbers Ra_B and Ra_W based on the amounts of bottom heating and internal heating

$$Ra_B = \left\langle \frac{\bar{g}(r)\bar{\alpha}(r)\Delta T_{sa}d^3}{\bar{\nu}(r)\bar{\kappa}(r)} \right\rangle \quad \text{Bottom heating} \quad (5a)$$

$$Ra_W = \left\langle \frac{\bar{g}(r)\bar{\alpha}(r)Qd^5}{\bar{\nu}(r)\bar{\kappa}(r)k} \right\rangle \quad \text{Internal heating} \quad (5b)$$

the dissipation number Di associated with effects of compressibility

$$Di = \ln \left(\frac{\bar{T}_{bot}}{\bar{T}_{top}} \right) \quad (6)$$

and the inner to outer radius ratio r_{bot}/r_{top} . In (5) and (6), $\bar{\alpha}(r)$ is the thermal expansivity of the basic state, ΔT_{sa} is the superadiabatic temperature difference across the spherical shell, d is the thickness of the shell, $\bar{\nu}(r) = \mu/\bar{\rho}(r)$ and $\bar{\kappa}(r) = k/(\bar{\rho}(r)c_p)$ are the momentum and thermal diffusivities of the basic state, \bar{T}_{bot} and \bar{T}_{top} are the basic state temperatures at r_{bot} and r_{top} , respectively, the inner and outer radii of the shell. The angle brackets in (5) indicate volume averages, and the specific heat at constant pressure c_p is assumed to be a constant. The Rayleigh numbers in all of the solutions presented here are about 100 times the critical values of Ra for the onset of convection (Table 2). Though these values of Ra are, perhaps, an order of magni-

TABLE 2. Input Parameters for Particular Models

	90% HFB [†]		20% HFB [†]	
	Rigid Top	Shear-Stress-Free Top	Rigid Top	Shear-Stress-Free Top
<i>Mars</i>				
ϵ , W/kg	1.5×10^{-13}	1.5×10^{-13}	5.3×10^{-12}	5.3×10^{-12}
μ , Pa s	4.3×10^{21}	7.2×10^{21}	4.4×10^{21}	10.6×10^{21}
$(Ra_B + Ra_W)_{cr} \dagger$	1,675	957	15,062	6,292
$\ell_{cr} \ddagger$	4	3	5	4
$Ra_B + Ra_W$	164,180	100,700	1,516,100	629,170
$\frac{Ra_B}{Ra_B + Ra_W}$	0.756	0.756	0.085	0.085
$\Delta\theta, \Delta\phi^*$, deg	3.75	3.75	2.81	2.81
L^{**}	31	31	42	42
Δt^{***} , Ma	1.9	1.6	3.2	3.5
<i>Venus</i>				
ϵ , W/kg	2×10^{-13}	2×10^{-13}	5×10^{-12}	5×10^{-12}
μ , Pa s	24.8×10^{22}	45.2×10^{22}	19.6×10^{22}	51.8×10^{22}
$(Ra_B + Ra_W)_{cr} \dagger$	2,188	1,200	26,326	9,966
$\ell_{cr} \ddagger$	4	3	5	4
$Ra_B + Ra_W$	228,100	125,070	2,778,900	1,051,800
$\frac{Ra_B}{Ra_B + Ra_W}$	0.713	0.713	0.090	0.090
$\Delta\theta, \Delta\phi^*$, deg	3.75	3.75	2.81	2.81
L^{**}	31	31	42	42
Δt^{***} , Ma	4.8	5.4	8.6	11.6

[†] HFB is the abbreviation for heated from below. 90% HFB refers to cases that are predominantly (approximately 90%) heated from below. 20% HFB refers to cases that are mostly heated from within (i.e., approximately 20% heated from below).

[‡] $(Ra_B + Ra_W)_{cr}$ is the minimum critical total Rayleigh number $Ra_B + Ra_W$ (see equation (5)) which occurs at spherical harmonic degree ℓ_{cr} .

* $\Delta\theta$ and $\Delta\phi$ are the latitudinal and longitudinal grid spacings, respectively.

** L is the truncation value for the spherical harmonic series, i.e., the maximum spherical harmonic degree and order are both equal to L .

*** Δt is the average time step for the numerical time integration of equation (4).

tude smaller than the range of Ra appropriate to the mantles of Venus and Mars, they insure that our solutions are reasonably resolved. The inner to outer radius ratio of Mars is taken to be 0.55, similar to that of the Earth's whole mantle. Venus' mantle is probably slightly thicker [Stevenson *et al.*, 1983] and $r_{bot}/r_{top} = 0.514$ is used. The model for Mars with a small core has an inner to outer radius ratio of 0.2.

The dissipation number in the Venus model calculations is 0.5, similar to the value of Di for the Earth's mantle. Venus is a relatively large terrestrial planet; effects of mantle compressibility are important as measured by the order unity value of Di . The dissipation number for the Martian mantle is very small, and we take $Di = 0$ in the Mars models. The limit $Di = 0$ is the Boussinesq limit. Effects of mantle compressibility are not important in a relatively small planet like Mars.

RESULTS

A total of eight simulations are generated for Mars and Venus models appropriate to the geologic present. For each planet, simulations are run for the spherical shell predominantly heated from within and heated from below; for each of these two heating modes, calculations are made for a rigid and a shear-stress-free upper boundary. As discussed earlier, the rigid outer boundary is the condition most relevant to Mars and Venus, while the free outer boundary results are included to facilitate assessment of the effects of the rigid

boundary condition on convection. The model for Mars with a small core has a rigid upper boundary and is mostly heated from below, corresponding to an intense heat pulse or a heat flow from a very hot core during or just subsequent to core formation. All the simulations (except as noted later) are started with random perturbations to the entropy of the conductive state. Entropy perturbations with spherical harmonic degree $\ell \leq 9$ are initialized randomly; perturbations with $\ell > 9$ are initially zero.

Three-Dimensional Structure of Convection

Radial velocity contours at middepth in the shells are shown in Figure 2 for both Mars and Venus models that are predominantly heated from within. In both models, between 16% and 20% of the surface heat flow originates in the core. (Since the solutions are time dependent, the proportion of basal heating is not constant and varies a few percent around a mean value.) Radial velocities are shown for both rigid and shear stress-free upper boundary conditions. Meridional cross sections of total entropy, shown in Figure 3 for the same cases as in Figure 2, provide a view of the vertical structure of the flows, at least within one meridional plane. In these mainly heated-from-within models of convection in the mantles of Mars and Venus, upwellings are generally in the form of cylindrical-like plumes, while downwellings are both sheet-like and cylindrical. There are instances in which upwelling plumes are highly elongated in one direction and other instances in which upwelling plume centers

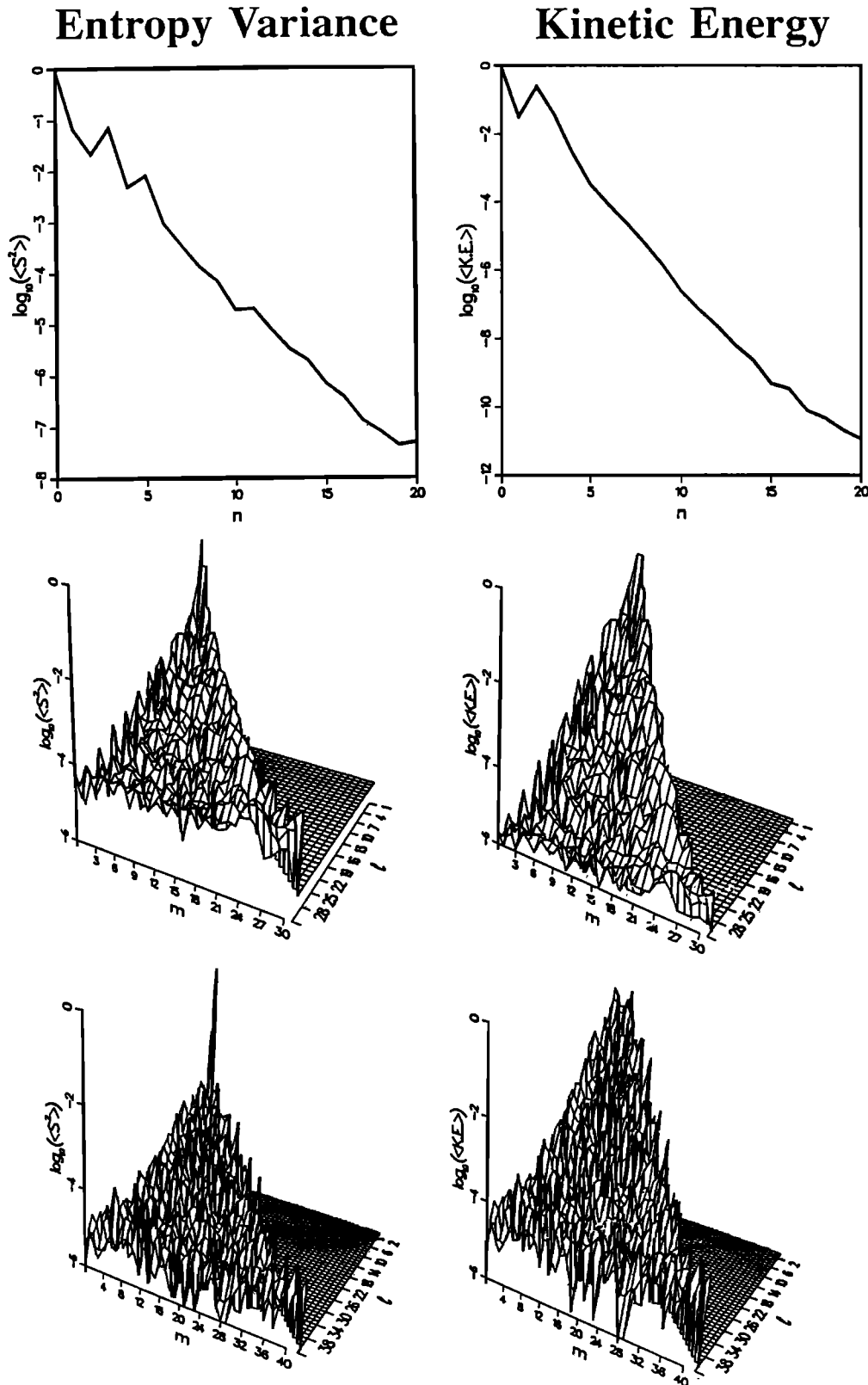


Fig. 1 Characteristic power spectra for the Chebyshev (top) and spherical harmonic expansions of dependent variables. Spherical harmonic power spectra are shown for both the truncation levels ($L=31$ and $L=42$) used for 90% (middle) and 20% (bottom) heated-from-below (HFB) cases. The Chebyshev degree (or wave-number) is n ; the spherical harmonic degree and order are ℓ and m , respectively. Entropy variance $\langle S^2 \rangle$ and kinetic energy $\langle KE \rangle$ [see Glatzmaier, 1988] are both shown to demonstrate the resolution of the energy and momentum fields. The power is normalized by the maximum power.

TABLE 3. Output Parameters

	90% HFB†		20% HFB†	
	Rigid Top	Shear-Stress-Free Top	Rigid Top	Shear-Stress-Free Top
$\langle q \rangle_{top}^*$, W	1.06×10^{12}	1.12×10^{12} ^{Mars}	2.48×10^{12}	2.60×10^{12}
v_{max}^{**} , cm/yr	1.70	1.52	0.98	0.85
$\langle q \rangle_{top}^*$, W	7.5×10^{12}	7.6×10^{12} ^{Venus}	2.03×10^{13}	2.1×10^{13}
v_{max}^{**} , cm/yr	1.13	1.07	0.69	0.57

† HFB is the abbreviation for heated from below. See note to Table 2.

* $\langle q \rangle_{top}$ is the total surface heat flow.

** v_{max} is the maximum velocity.

TABLE 4. Input and Output Parameters for the Mars Small Core Model (90% HFB, Rigid Top)

Parameter	Value
r_{top} , km	3200
r_{bot} , km	640
$\bar{\rho}$, kg/m ³	4130
T , K	1500
M_{core} , kg	7.14×10^{21}
α , K ⁻¹	2×10^{-5}
ΔT_{ra} , K	2000
ϵ , W/kg	1×10^{-13}
k , W/K/m	4.96
μ , Pa s	2.81×10^{22}
c_p , kJ/K/kg	12
$(Ra_B + Ra_W)_{cr}$ (at $\ell = 1$)†	3615
$(Ra_B + Ra_W)_{cr}$ (at $\ell = 2$)†	3613
$(Ra_B + Ra_W)$	355,450
$\frac{Ra_B}{Ra_B + Ra_W}$	0.786
Δr_{mid}^* , km	100
Δr_{top} , Δr_{bot}^* , km	4
$\Delta \theta$, $\Delta \phi^*$, deg	3.75
N^{**}	20
L^{**}	31
Δt^{**} , Ma	4.2
$\langle q \rangle_{top}^\ddagger$, W	4.88×10^{11}
v_{max}^\ddagger , cm/yr	0.87

HFB is the abbreviation for heated from below. See note to Table 2.

† $(Ra_B + Ra_W)_{cr}$ is the critical total Rayleigh number which occurs at the specified values of ℓ .

* Refers to resolutions.

** Defined in previous tables.

‡ See note to Table 3.

are connected by regions of weaker upwelling. Upwelling plumes are more numerous when the outer boundary is rigid as compared with shear stress-free. It is also well known that at the onset of convection, convection cell wavelengths are smaller for rigid boundaries than for shear-stress-free boundaries [Chandrasekhar, 1961]. This is possibly because viscous resistance and dissipation are greater in the upper boundary layer when the top is rigid, causing convection cells to assume a smaller wavelength in order to reduce the net viscous resistance per cell volume. There are about 13 upwelling plumes in the Mars model with the rigid upper boundary and about 20 plumes in the Venus model with the

rigid upper boundary. This implies that the effects of compressibility may increase the number of upwelling plumes. This is possibly due to partial stabilization of the lower portion of the shell by compressive stratification, leading to an effectively narrower unstable portion of the layer and thus smaller wavelength convective features. However, it is also possible that the difference in the number of plumes reflects differences in the random initial conditions. The particular meridional cross sections of total entropy in Figure 3 emphasize the downwelling sheets (and plumes) that originate as negatively buoyant instabilities from the upper thermal boundary layer. The downwelling sheets in the rigid top cases have less regular horizontal structure than in the stress-free top cases, i.e., with a rigid upper boundary the downwelling sheets tend to be comprised of linked downwelling plumes. In contrast, the downwelling sheets for the stress-free top cases have smoother lateral structure, almost zero velocity gradient parallel to the sheets, and tend to be longer (see also Figures 7 and 8).

Figures 4 and 5 show results similar to the first two figures but for Mars and Venus models in which 91 to 95% of the surface heat flow comes from the core. The upwelling flow in these mainly bottom-heated models is dominated by a few large plumes. Again, there are fewer upwelling plumes when the upper boundary is shear stress free as compared with when it is rigid. There are no obvious effects of compressibility on the number of plumes, as indicated by the similar numbers of plumes in the Mars and Venus models. This may be due to the large temperature drop across the lower thermal boundary layer which makes the stabilization due to compressibility negligible. The final state of the Venus case with a free top has a dominant $\ell = 2$ signature (hence only two plumes) even though the least stable mode at the onset of convection is at $\ell = 3$ (Table 2). The downwellings are all in an interconnected network of sheets; there are no cylindrical plume-like downwellings when heating is mainly from below as there are when internal heating dominates. However, as in the predominantly heated-from-within cases, the downwellings have more plume-like concentrations when the upper surface is rigid than when it is stress free. The particular meridional cross sections of total entropy emphasize the upwelling plumes, in contrast to the internally heated cases wherein the meridional cross sections

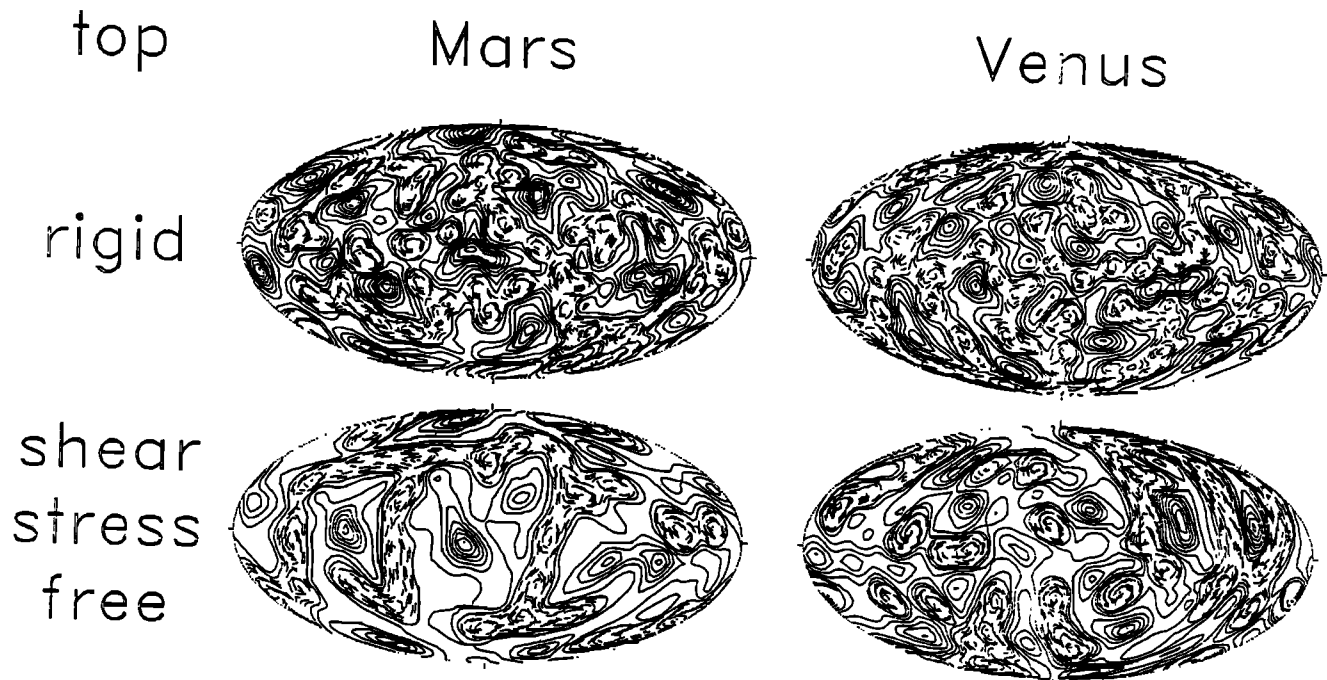


Fig. 2. Radial velocity contours at middepth in the shells of Mars and Venus models with approximately 20% of the outer surface heat flow originating from below. Results are shown for both rigid and shear-stress-free outer boundary conditions. The contours are plotted on a Hammer-Aitoff equal-area projection. Velocities typically range from about -3×10^{-10} to 1×10^{-10} m/s. Contour intervals are constant.

feature the downwellings. The upwelling plumes originate as buoyant instabilities from the hot lower thermal boundary layer. They transport most of the core heat flux across the spherical shell to the upper surface; in these predominantly heated-from-below models the plumes therefore transport the bulk of the total heat flow. When the plumes interact with the upper boundary, they flatten and spread laterally away from the upwelling center. In these mainly heated-from-below cases, the relatively small number of plumes in the Mars and Venus models with rigid upper boundaries may have implications for the concentration of volcanic activity in relatively few centers on Mars and Venus.

Figure 6 shows radial velocity contours at different depths for the predominantly basally heated models. For all four cases the upwelling plumes undergo little structural change with depth. When the top boundary is shear stress free, the downwelling sheets also appear essentially the same at different radii (aside from apparent thickening, which is more due to the fact that the surface area of the map projection decreases with depth). In contrast, when the top boundary is rigid, the downwelling sheets experience considerable change with depth, going from narrow and concentrated near the top of the shell to broad and dispersed near the bottom (even when accounting for the area of the map projection). Furthermore, when the upwelling plumes impinge on the upper boundary, they do not flatten and spread out into the boundary layer as evenly when the top boundary is rigid as when it is free. This is perhaps what leads to the less regular structure of the downwelling sheets in the rigid top cases, since the sheets initiate with an almost dendritic structure. The rigid boundary appears responsible for establishing a nonaxisymmetric boundary layer structure around the plumes, perhaps by some downwelling instabil-

ity. This may have relevance for the radial fractures on the Tharsis rise on Mars, since there appears to be a spoke-like configuration of narrow downwelling currents centered on the upwelling plumes and there is necessarily extensional strain between these currents.

Time Dependence

The temporal evolutions of the Mars and Venus models are shown in Figures 7 and 8 for the mainly internally heated cases and in Figures 9 and 10 for the mainly bottom-heated cases. The principal feature of the bottom-heated cases is the large reduction in the number of plumes with time through the process of plume merging. This is particularly evident in the models with a free upper boundary in which the number of plumes reduces from as many as eight in the Venus case to just two during the course of the evolution. An especially interesting example of plume merging is seen in the mainly bottom-heated Venus model with a rigid upper boundary (Figure 10), wherein adjacent plumes separated by a downwelling sheet at 96 Ga, have broken the sheet at 132 Ga, and have merged by 154 Ga. Although the rigid and the free top cases have different final states, their manner of plume fusion is the same. This probably occurs because the plumes' temporal behavior is controlled by fusion at their bases in the lower boundary layer; since the characteristics of the lower boundary (shear-stress-free) are the same for all cases, the time-dependent behavior of the plumes is similar for all cases.

The time histories of the mainly internally heated models are more difficult to describe because of the more complex character of the solutions; compared to the mainly bottom-heated cases, the mainly internally heated cases

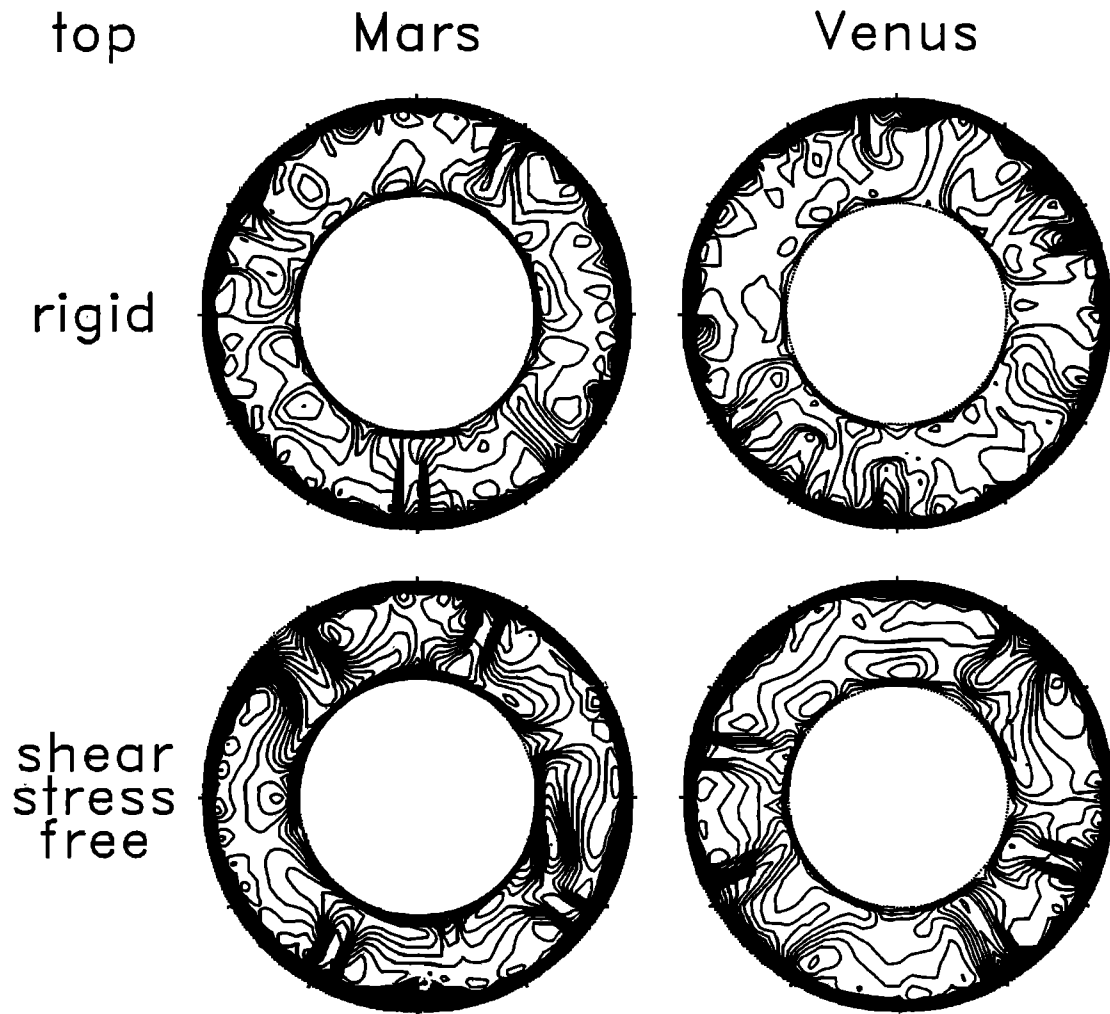


Fig. 3. Meridional cross sections of total entropy for the models of Figure 2.

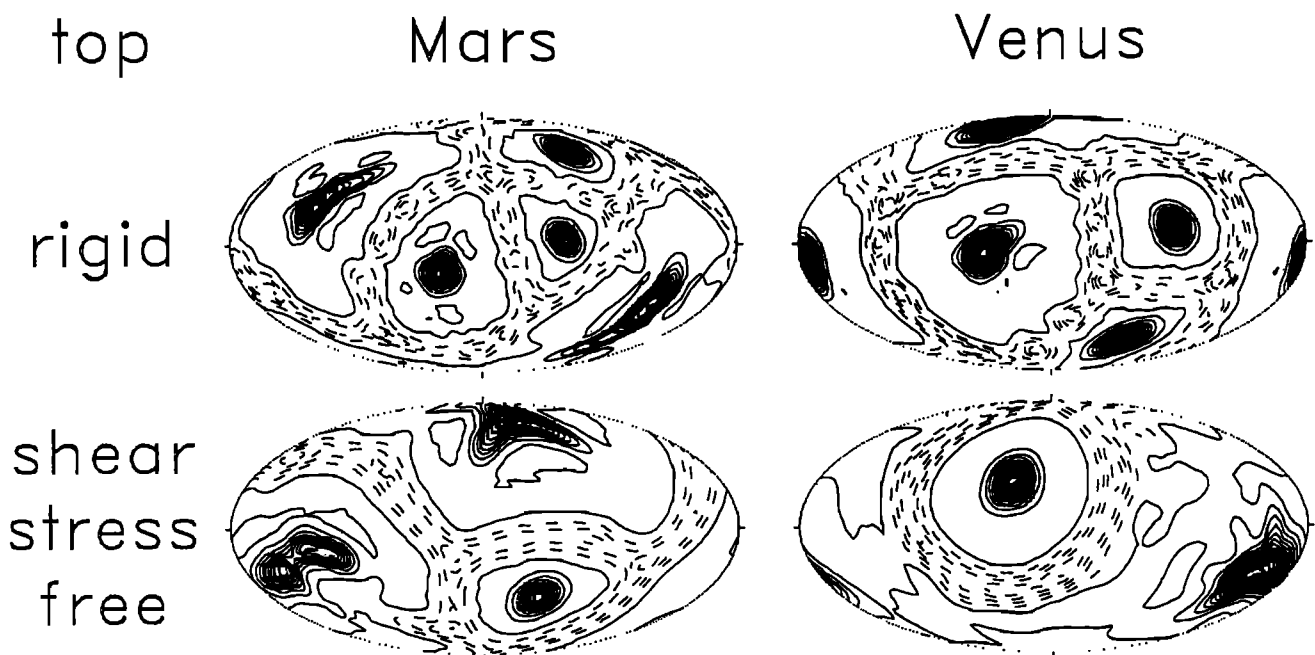


Fig. 4. Similar to Figure 2 but for Mars and Venus models in which approximately 90% of the outer surface heat flow derives from the core. Velocities typically range from -2×10^{-10} to 5×10^{-10} m/s.

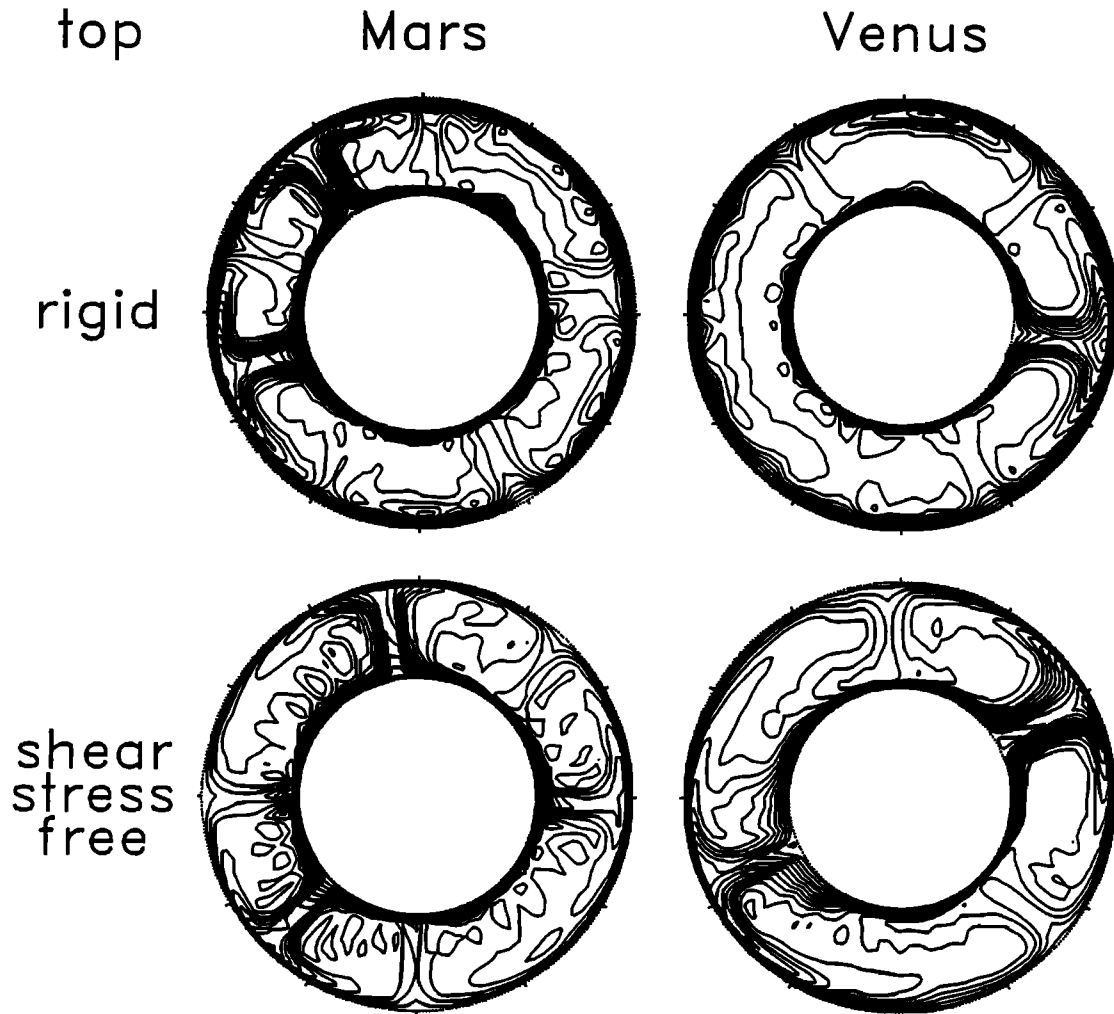


Fig. 5. Meridional cross sections of total entropy for the models of Figure 4.

have smaller and weaker plumes and a more complex network of downwellings with both sheets and plumes. Plume merging also occurs in the mainly heated-from-within models, but a more striking feature of the time development is the evolution of the descending sheets and plumes. Descending sheets lengthen and change their shape by attaching descending plumes; the sheets also shorten and change shape by breaking off cylindrical concentrations of downwelling. The changing morphology of the descending sheets, rather than the changes in the number of plumes, is the major characteristic of the time development of spherical shells that are mainly heated from within. Because the downwelling sheets emanate from different boundaries for the rigid and free top cases, the temporal evolution of the sheets is different for these cases. In the free top case, the sheets tend to come together into more extensive and long-lived features, while in the rigid top case, the sheets are relatively short in horizontal extent and have a greater frequency of breakup. This probably relates to the laterally nonuniform horizontal structure of the upper boundary layer discussed above. The final time steps shown in the above figures are believed to represent results that are quasi-steady in the sense that no further significant qualitative changes in the convective patterns would probably occur if the integrations were carried further in time.

Aspects of the temporal evolutions of the Mars and Venus models may have relevance to the thermal, tectonic, and dynamic histories of the planets. The relatively slow drift and/or immobility of strong upwelling plumes may imply that large mantle plumes leading possibly to features like Tharsis are very long-lived and may move so slowly that the planet's rotation will adjust to their perturbation of the planet's moment of inertia much faster than the plumes themselves can move. Since plumes cause dynamic uplift, their net geoid anomaly and thus their contribution to the planetary moment of inertia is positive. Therefore one can always expect to find the largest dynamic uplift along the equator. The temporal behavior of the downwelling sheets may have some bearing on how the tectonics of Mars and Venus compare with the tectonics of the Earth. The modelling results for the mainly internally heated cases suggest that a free upper boundary is conducive to extensive and temporally durable linear systems of subduction, while the rigid upper boundary is not. Thus for the Earth, the free motion of the plates facilitates convective currents that can best keep the plates moving. However, for a planet with an immobile lithosphere, long durable subduction zones that could break up the lithosphere would be unlikely to form. Other physical processes not included in our model would be required to break up an immobile planet-wide lithosphere

Mars (90% H.F.B.)

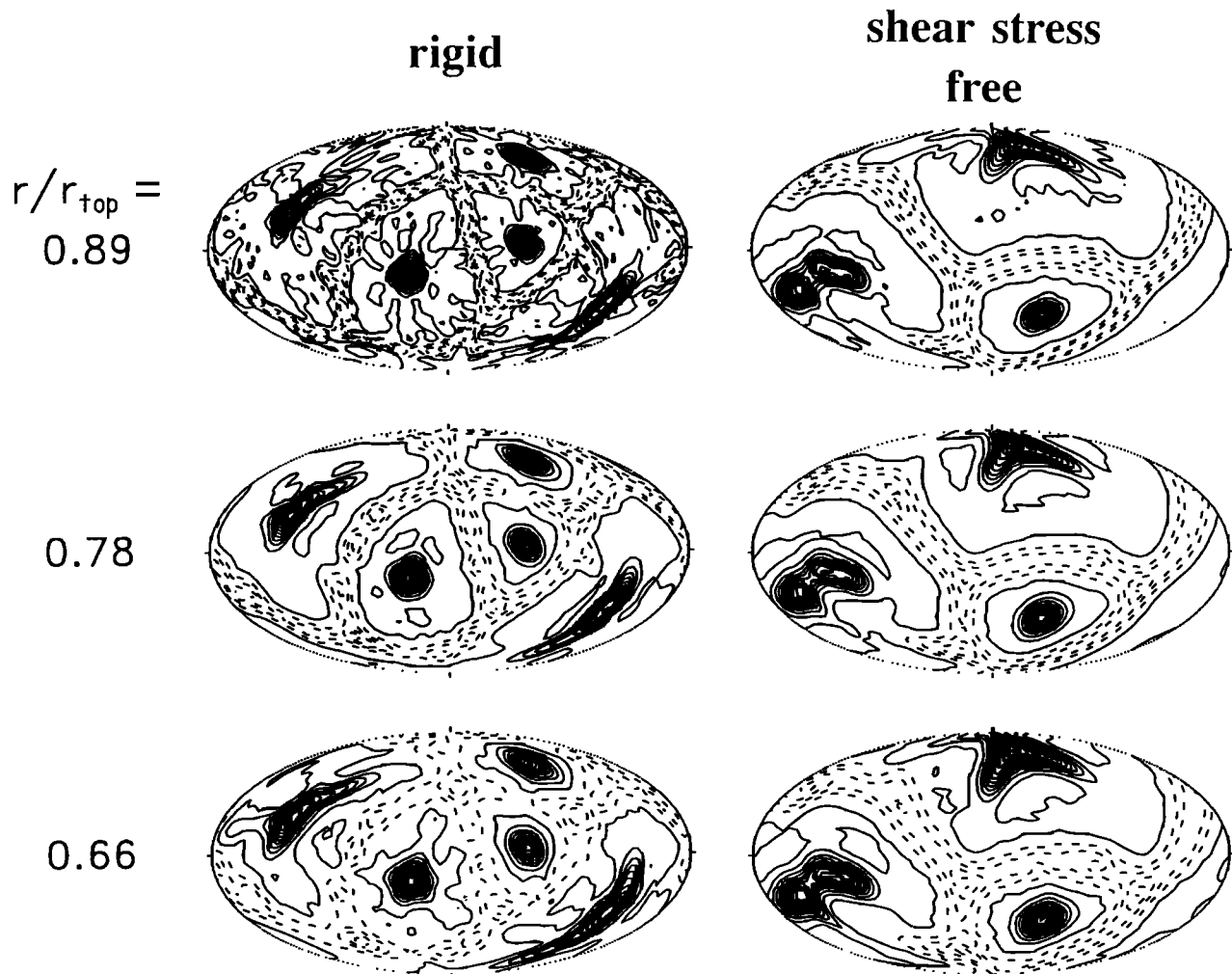


Fig. 6a. Radial velocity contours at different depths for the Mars models that are predominantly (approximately 90%) heated from below with both rigid and shear-stress-free upper boundaries. See Figure 4 for typical velocity ranges.

if indeed that is possible. Multiple, mobile plates may have to exist from the beginning if they are to occur at all.

The time dependence of the solutions presented above is also evident in the plots of the volume averaged kinetic energy in the shell as a function of time and the corresponding power spectra in frequency space shown in Figures 11–14. Most of the cases show a significant periodicity. This is most clear in the cases whose kinetic energy time series are not modulated by a long-period oscillation. While the Mars models show a decrease in dominant frequency in going from a rigid to a free top boundary for both heating modes, the Venus cases show just the opposite behavior. Generally, the dominant frequencies of the periodicities are within factors of 2 or 3 of the characteristic overturn frequency $v_{max}d/\pi\kappa(r_{bot})$ (where v_{max} can be found in Table 3). The Venus free top case with mostly bottom heating has only two plumes during its periodic episode, which may account for the fairly pure periodic signature. However, the periodic oscillation also appears to be overstable until it is disrupted

just prior to the end of the time series. Three of the four cases with mainly internal heating are significantly periodic even though such a heating mode is characterized by a complex pattern evolution. In all the cases the variability in the volume averaged kinetic energy is at the 10% level.

Temperature Profiles

Radial profiles of spherically averaged temperature for the Mars and Venus models are shown in Figure 15. The largest temperature variations occur in thermal boundary layers at the inner and outer surfaces of the spherical shells. When only 20% of the surface heat flow originates from below, the temperature change across the lower thermal boundary layer is smaller than the temperature change across the upper thermal boundary layer, while the reverse is true when 90% of the surface heat flow originates from below. These temperature changes are consistent with overall energy balances for the model spherical shells, taking into account dif-

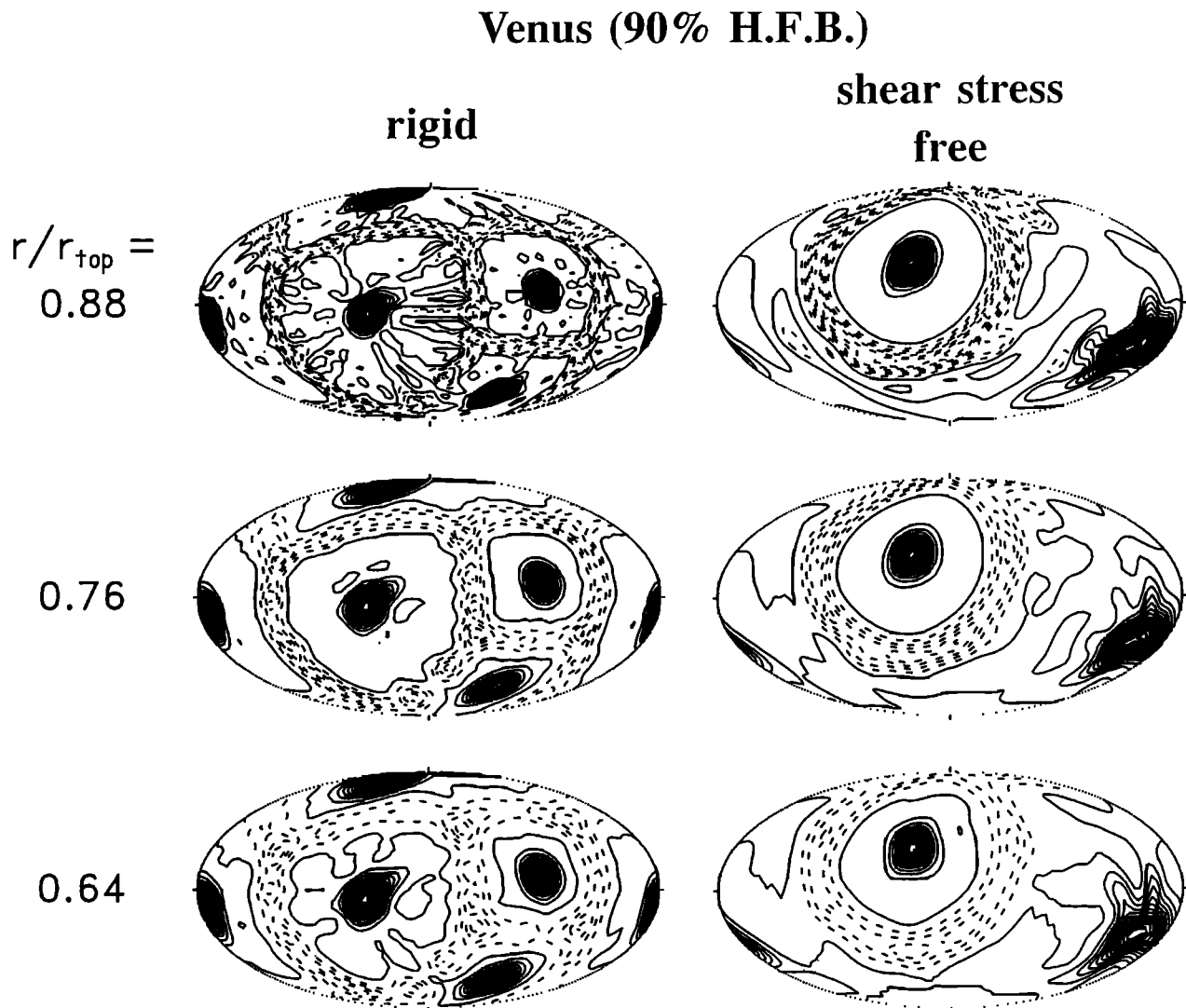


Fig. 6b. Radial velocity contours at different depths for the Venus models that are predominantly (approximately 90%) heated from below with both rigid and shear-stress-free upper boundaries. See Figure 4 for typical velocity ranges.

ferences in surface areas of the upper and lower boundaries, heat fluxes at the surfaces, internal rates of heat production and boundary layer thicknesses.

In the Mars models of Figure 15, the interior (external to the boundary layers) temperatures are significantly subadiabatic, i.e., the interior temperatures decrease with depth. In the Venus models of Figure 15, interior temperatures are also subadiabatic. Nevertheless, interior temperatures in three of four of the Venus cases increase with depth because the relatively large adiabatic temperature gradient in the Venus models dominates over the subadiabaticity. The Venus case with 20% heating from below and a free upper boundary is so strongly subadiabatic in its interior that the interior temperature is nearly isothermal. The adiabatic temperature gradient in the Mars models is zero; thus the subadiabaticity of the interior is more directly observable in the temperature profiles.

It can be seen in Figure 15 that the effect of the rigid upper boundary is to increase the interior temperature compared with the free upper boundary. The rigid upper boundary

reduces the mean velocity of the upper thermal boundary layer (compared with the free upper boundary) and thus retards cooling of the shell since heat flow out of the shell is proportional to $\sqrt{v_{bl}}$, where v_{bl} is the boundary layer velocity [Turcotte and Schubert, 1982]. To compensate for the less efficient cooling of the shell, the temperature drop across the boundary layer is larger than for the free top case, which leads to greater temperatures in the interior of the shell when the upper boundary is rigid. This result may have implications for the interior temperatures of Earth and Venus. If these planets are similar in all respects other than the occurrence of plate tectonics on Earth, then mantle convection in the Earth takes place with a free upper boundary while mantle convection in Venus takes place with a rigid upper boundary. Not only does Venus have a higher surface temperature than the Earth, but according to the above results it would also have a hotter interior temperature.

Figure 15 also shows that the interiors of the models with predominantly internal heating are significantly hotter than the interiors of the mainly bottom-heated models. This is

Mars (20% H.F.B.)

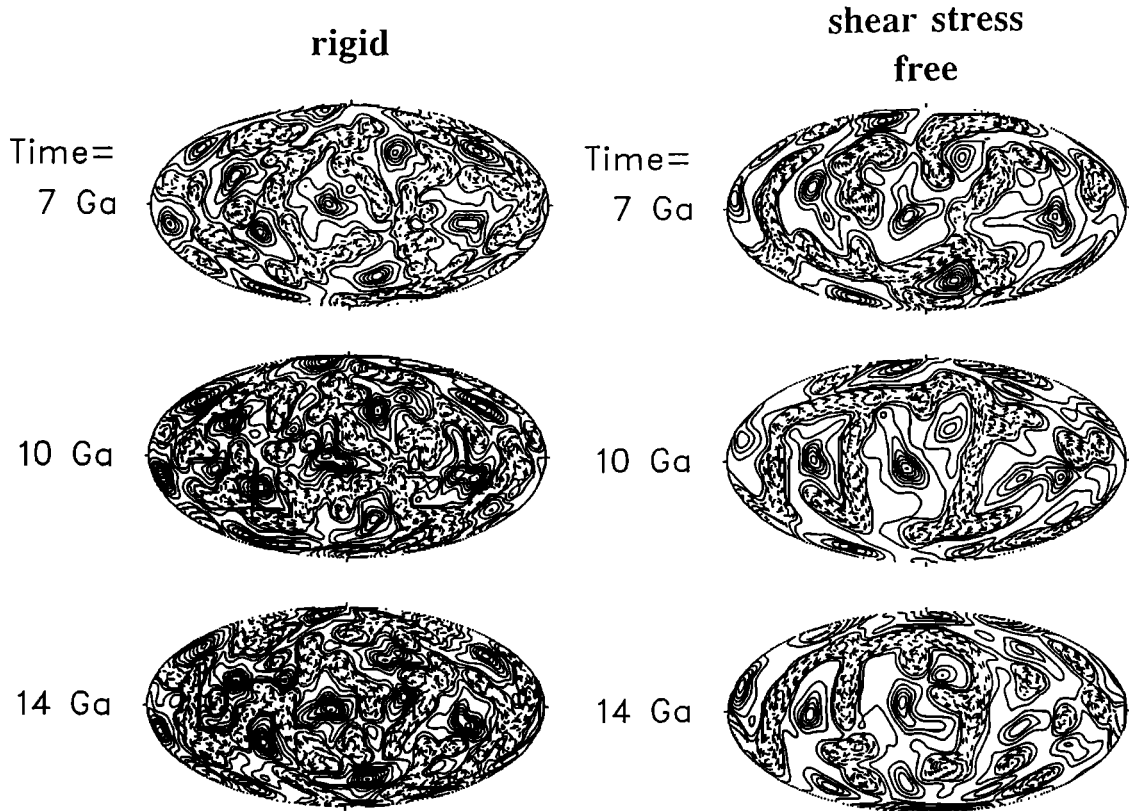


Fig. 7. Radial velocity contours at middepth for different times for the Mars models that are predominantly heated from within (i.e., approximately 20% heated from below) for both rigid and shear-stress-free outer boundaries. See Figure 2 for typical velocity ranges.

Venus (20% H.F.B.)

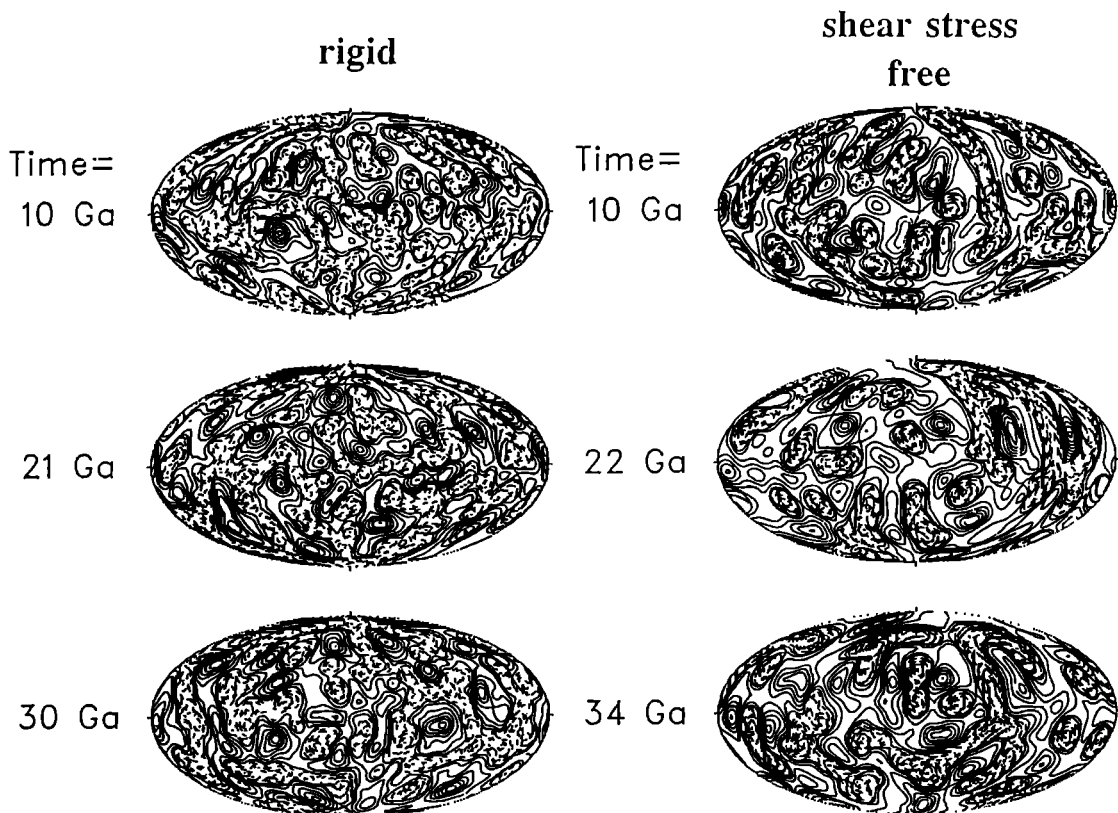


Fig. 8. Similar to Figure 7 but for Venus models that are mainly heated from within.

Mars (90% H.F.B.)

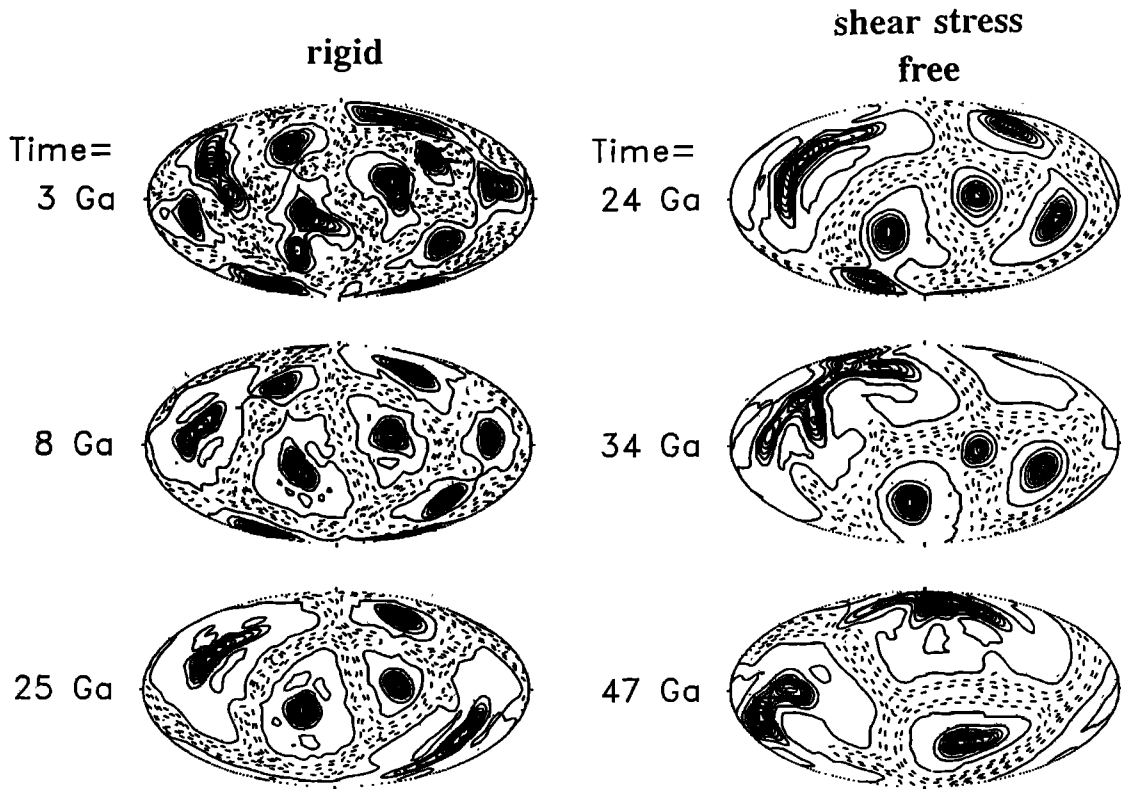


Fig. 9. Similar to Figure 7 but for Mars models which are mostly heated from below. See Figure 4 for typical velocity ranges.

Venus (90% H.F.B.)

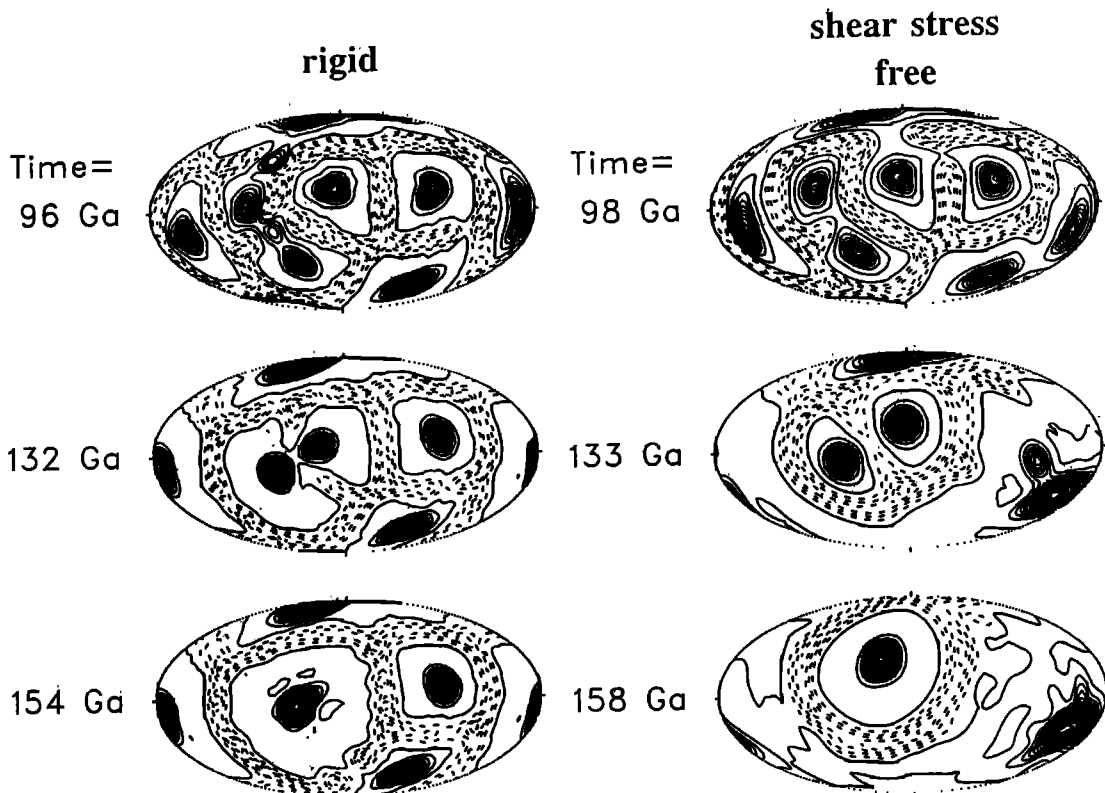


Fig. 10. Similar to Figure 8 but for Venus models that are predominantly heated from below. See Figure 4 for typical velocity ranges.

Mars (20% H.F.B.)

rigid

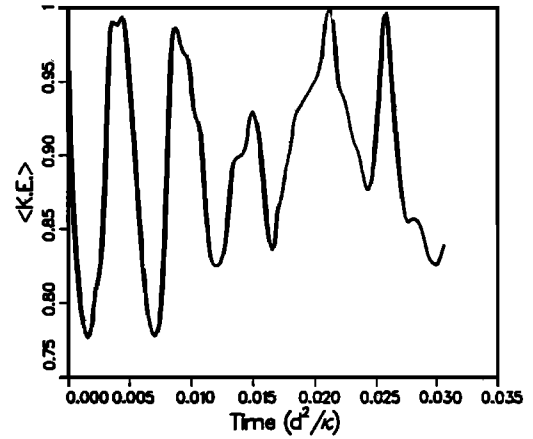
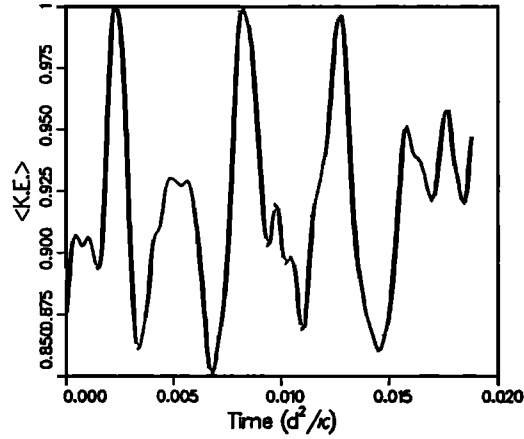
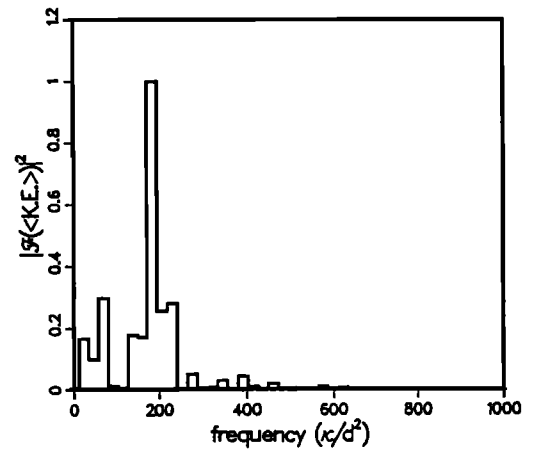
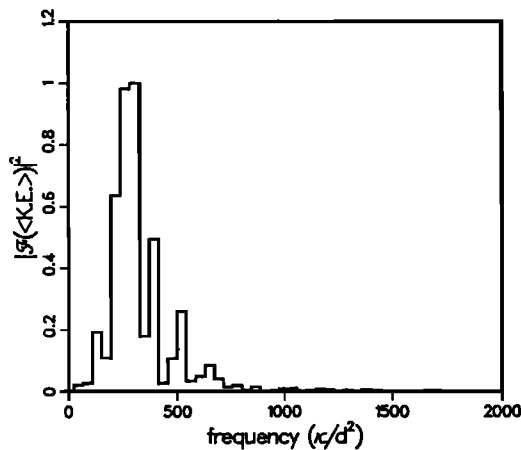
shear stress
freetime
seriesFourier
power
spectrum

Fig. 11. Volume-averaged kinetic energy versus time and the corresponding Fourier power spectrum of volume averaged kinetic energy in frequency space for the cases of Figure 7. Time is nondimensionalized by d^2/κ and frequency is nondimensionalized by κ/d^2 . Kinetic energy is normalized by its maximum value. The power spectral density is a maximum at a frequency of 302.2 for the rigid case and 184 for the shear-stress-free case.

a consequence of the larger total surface heat flow in the predominantly heated-from-within models which have the same boundary temperatures as the bottom-heated models.

Heat Flow and Energy Budgets

The heat flow and energy budgets of the models are illustrated by the radial profiles of spherically averaged quantities in Figures 16–19. The figures contain radial profiles of surface-integrated conductive, advective and total heat flow. Surface-integrated conductive heat flow is $-4\pi r^2 k(\partial/\partial r)(\overline{T} + \overline{T}')$ and surface-integrated advective heat flow is $4\pi r^2 \overline{\rho T v'_s s'}$ (where the overline indicates spherically averaged). Also included in the figures are radial profiles of individual heating terms in the energy (entropy)

equation that contribute to $4\pi r^2 \overline{\rho T (\partial s'/\partial t)}$; these terms are internal heating, viscous heating, diffusive heating and advective heating (where advective heating is the negative of the advection term on the right side of (4)). There is no viscous heating in any of the Mars models since the dissipation number is zero in these models. Conduction is the main heat transfer mechanism in the boundary layers, while advection predominates in the interiors. In the Mars models, conductive heat transfer in the interior is actually downward because of the subadiabaticity of the interiors of these models. Conductive heat transfer in the interiors of the Venus models is small but always directed upward, as a consequence of the contribution of upward conduction along the adiabat which offsets the effect of subadiabaticity in the interiors of the Venus models. Compressibility has an important effect on the total heat flow in the mainly heated-from-below mod-

Venus (20% H.F.B.)

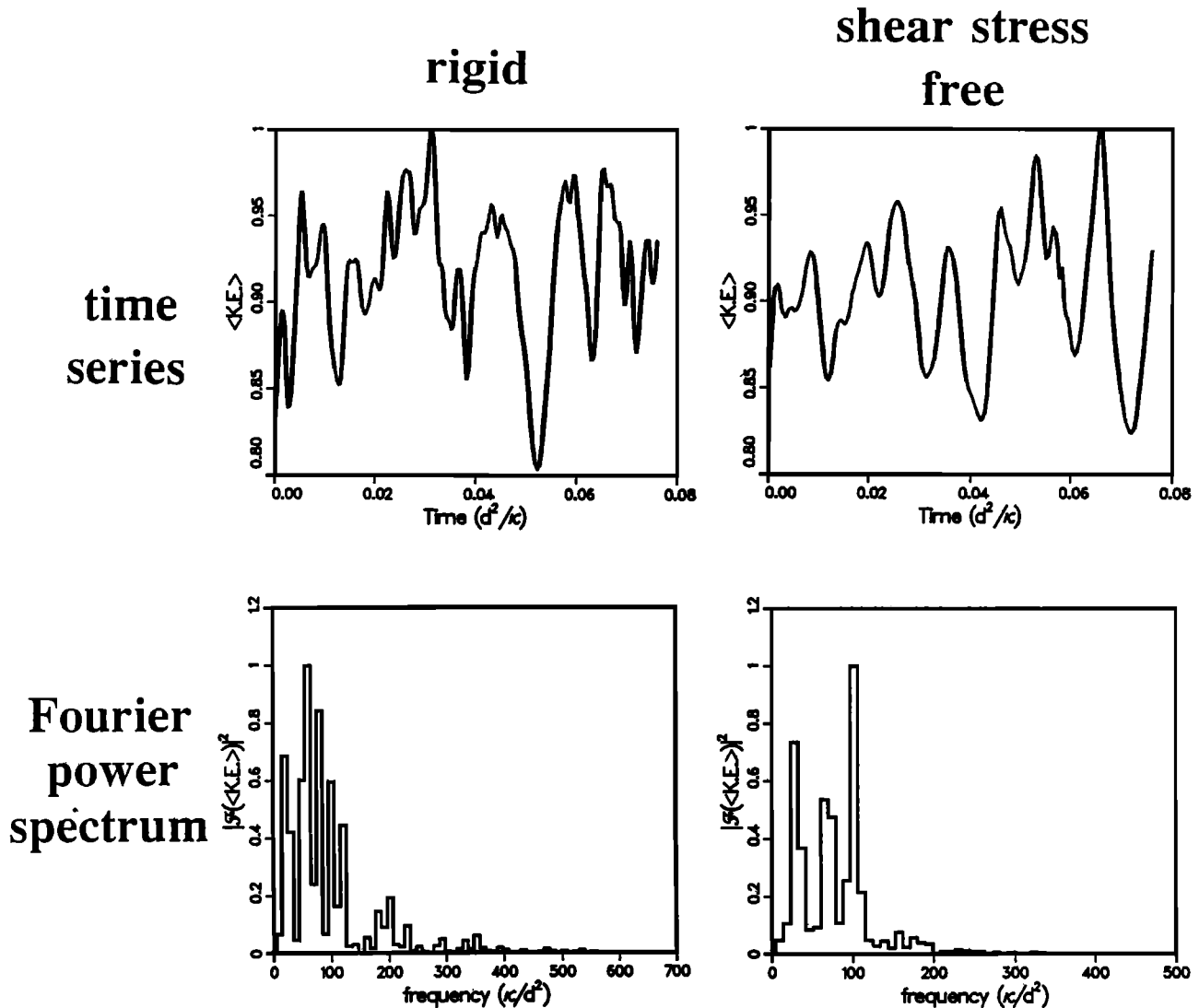


Fig. 12. Similar to Figure 11 for the cases of Figure 8. For the Venus models $\kappa = \kappa(r_{bot})$. The frequencies of maximum spectral power are 60.4 (rigid) and 101.6 (shear stress free).

els. As can be seen in the Venus cases, total heat flow both increases and decreases with radius; this occurs because although total viscous and adiabatic heatings cancel (in steady state), they are not uniformly distributed and thus represent heat sources and sinks that vary in magnitude with position. For example, viscous heating is most concentrated in the upper and lower boundary layers, as shown in the profiles of the heating terms for the Venus models.

The major contributions to the energy equation in the models arise from diffusive and advective heating (see also Glatzmaier [1988]). These terms predominate in the boundary layers and nearly cancel each other in the Mars models; in the Venus models the viscous heating causes the advective and diffusive heating of the boundary layers to be less than the corresponding cooling since all three terms nearly cancel each other. The heating terms in the interiors of the models are relatively small, especially in the

mainly heated-from-below cases. In the heated-from-within cases, advective cooling is the main mechanism to balance internal heat production in the interior. Viscous heating in the Venus models occurs mainly in the boundary layers; viscous heating in the upper boundary layer is enhanced by the rigid upper boundary. The rigid upper boundary also significantly modifies the magnitude and distribution of the diffusive cooling terms and the advective heating terms in the upper boundary layer; the Venus models provide particularly striking examples of this. The rigid boundary appears to retard heating and cooling of the boundary layer by slowing the deposition of heat into it by advection.

The differences in net surface heat flow between the predominantly internally heated cases and the mostly bottom heated cases is obviously due to the internal heat source (Table 3). Yet, even with this added energy source, the maximum velocity for the mainly heated-from-within cases

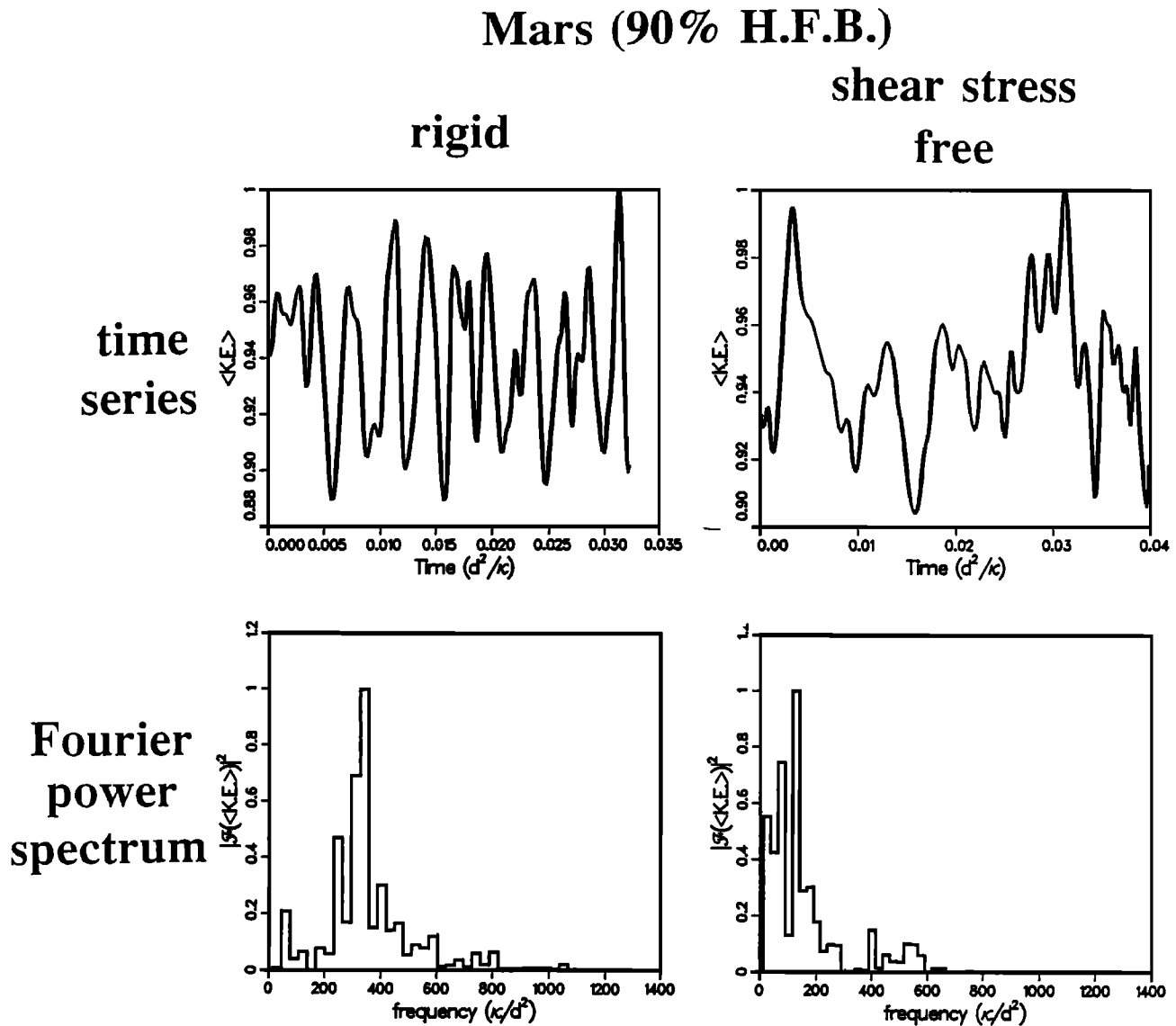


Fig. 13. Similar to Figure 11 for the cases of Figure 9. The frequencies of maximum spectral power are 340.2 (rigid) and 125.5 (shear stress free).

is less than for the predominantly heated-from-below cases. This probably occurs because upwelling velocities are the largest velocities in strongly bottom heated convection, and plumes tend to have smaller cross-sectional areas than the downwelling sheets and thus move faster to maintain essentially the same mass flux as the sheets.

Mars Small Core Model

Core size is another important factor in determining the number of convective plumes. With smaller cores there is a tendency toward larger wavelength convection cells [Zebib *et al.*, 1983] and thus fewer upwelling plumes. This is confirmed by the results of a simulation of convection in a model of Mars' mantle with a core radius 0.2 times the radius of Mars, a rigid top boundary, and between 85% and 90% of the surface heat flux originating in the core (Table 4). The variation in surface heat flow is due to time dependence. This model also has $Di = 0$ and a Rayleigh

number approximately 100 times the critical Ra . Figure 20 shows middepth radial velocity contours and isotherms in meridional cross section for this model. Similar figures for the primarily bottom-heated Mars model with a rigid top and $r_{bot}/r_{top} = 0.55$ are also shown to facilitate comparison with a model that has the present core size. The small core model has settled into a predominantly $\ell = 2$ convective pattern, even though the $\ell = 1$ and $\ell = 2$ modes are equally unstable at the onset of convection (Table 4). The $\ell = 2$ solution is relatively robust, having been arrived at twice with two different initial conditions, one with random perturbations to modes with $\ell \leq 4$ and one with random perturbations to modes with $\ell \leq 9$. Although the solution has a dominant $\ell = 2$ signature, it is not axisymmetric; i.e., the two plumes are not antipodal to each other. The heat flux through the surface of this model is one to two orders of magnitude less than that of the other models with a bigger core (Table 4). This is due to the significantly smaller net heat flux emanating from the core which has a surface

Venus (90% H.F.B.)

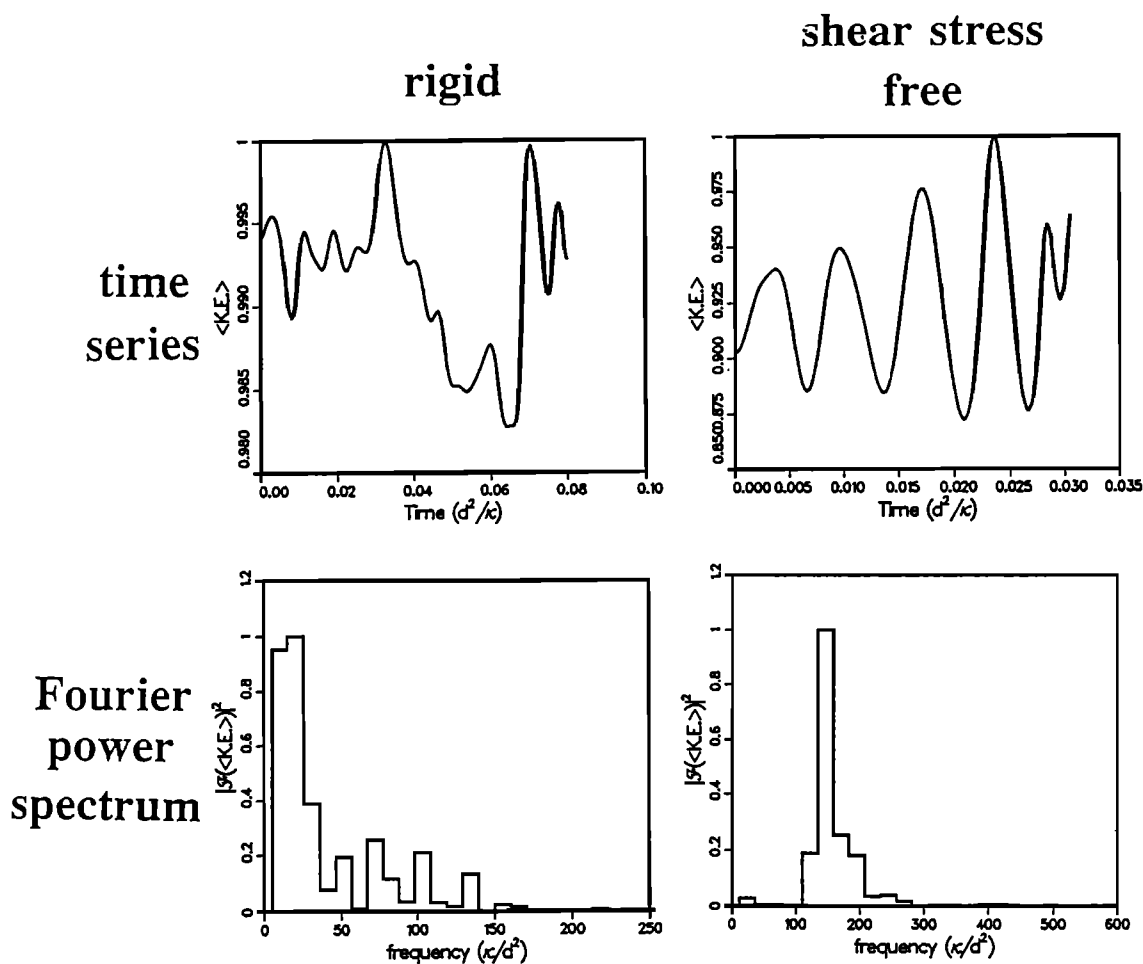


Fig. 14. Similar to Figure 12 for the cases of Figure 10. The frequencies of maximum spectral power are 20.7 (rigid) and 146.8 (shear stress free).

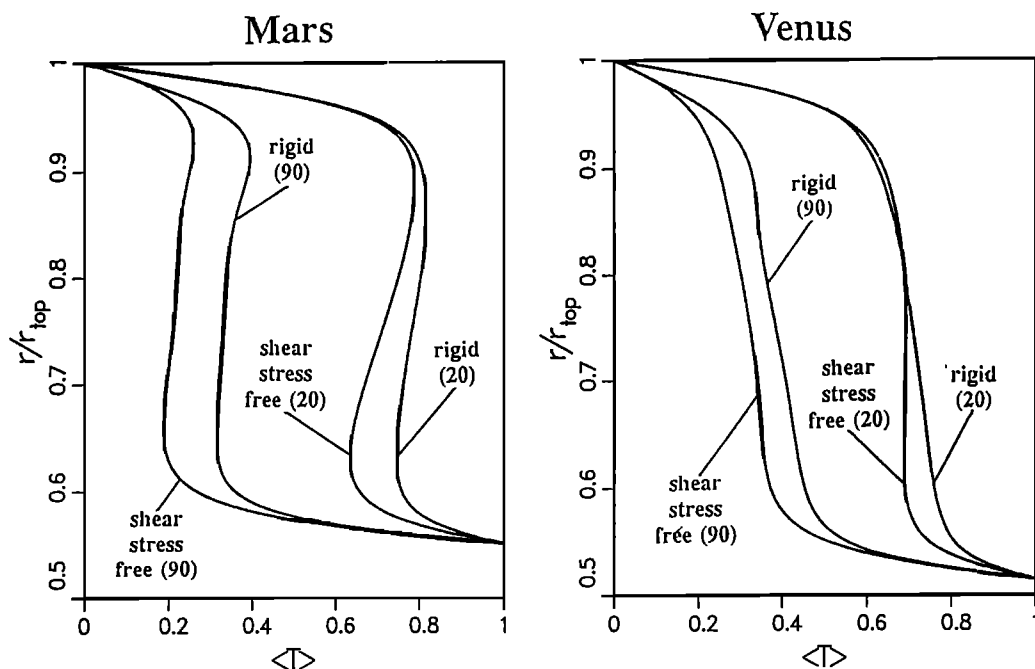


Fig. 15. Radial profiles of the spherically averaged temperature (T) for the models of Mars with a present core and Venus. Numbers in parentheses are the approximate percent of basal heating. Temperature profiles are all normalized so that the top temperature is 0, and the bottom temperature is 1.

Mars (20% H.F.B.)

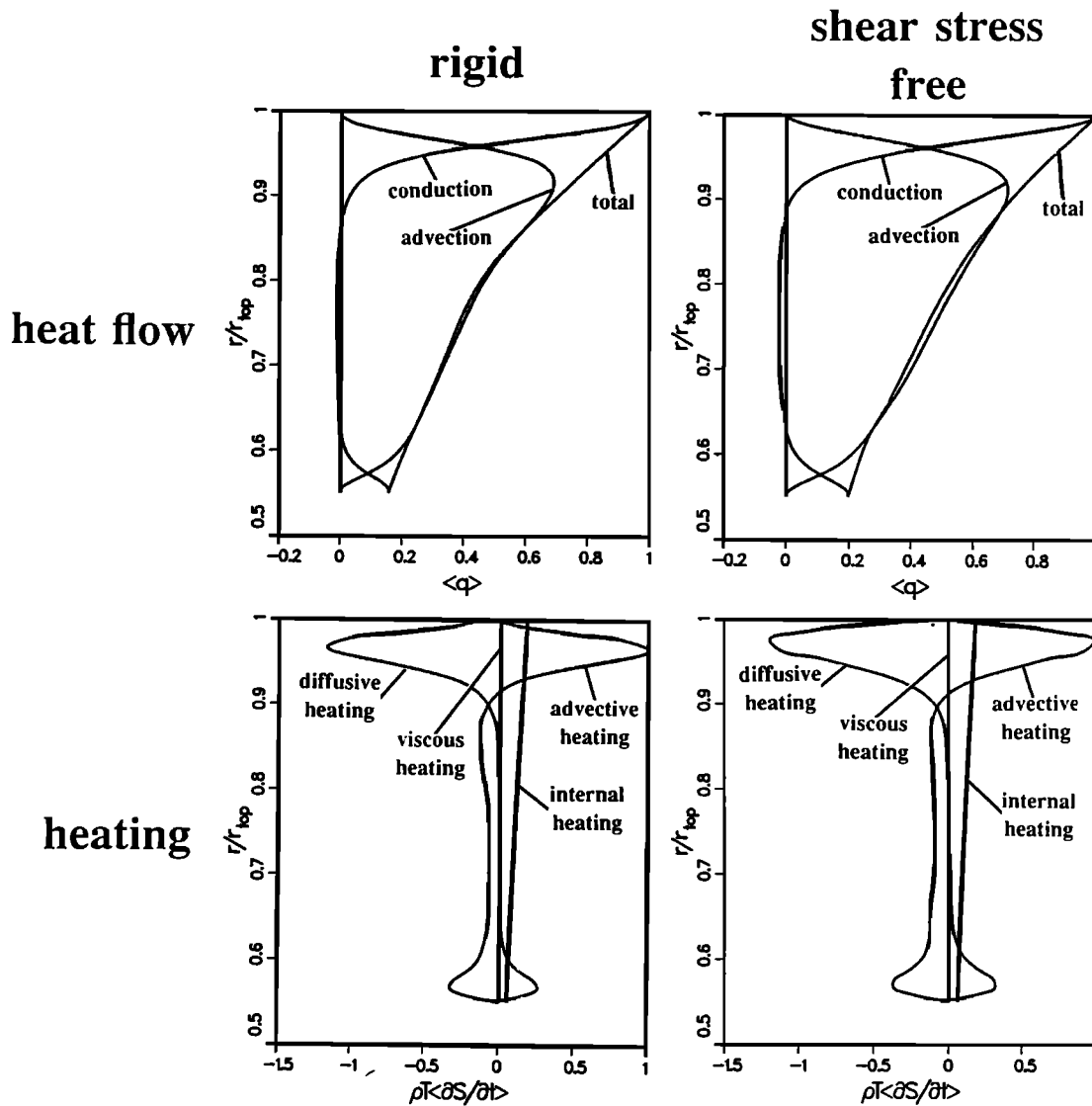


Fig. 16. Radial profiles of surface-integrated conductive, advective, and total heat flow and of the diffusive heating, internal heating, and advective heating contributions to the energy equation for Mars models in which approximately 20% of the surface heat flow originates in the core. There is no viscous heating in the Mars models.

area almost an order of magnitude less than the other Mars models. The maximum velocity is midway between the maximum velocities of the predominantly basally and internally heated cases of the other models.

Boundary Deflection and Topography

The dynamic topography generated by convective stresses on the upper boundary is readily calculated for the Venus and Mars models, since with a rigid top boundary, the hydrostatic head caused by topography is directly proportional to dynamic pressure. From the continuity of radial stress across the upper boundary we can write

$$\delta r = \frac{p'}{\Delta \rho_{top} \bar{g}(r_{top})} \tag{7}$$

(where δr is the amplitude of the topography and $\Delta \rho_{top}$ is the density contrast across the upper boundary) because the viscous radial stress is zero at a rigid boundary. We assume that $\Delta \rho_{top}$ is equal to $\bar{\rho}(r_{top})$. Calculation of topography with the assumption that a hydrostatic head balances dynamic pressure overestimates the topography, particularly on length scales smaller than the shell's outer radius since the rigid lithosphere would resist deformation by the convective stresses. This calculation of hydrostatic topography provides an upper limit to the possible topography.

Figure 21 shows topography at the upper boundary for the Mars model that is mainly heated from below and for the small core Mars model. The Venus models produce excessively large topographies, of the order of 20 km, due to the model viscosities which are probably 2 orders of magnitude too large (Table 2). According to boundary layer

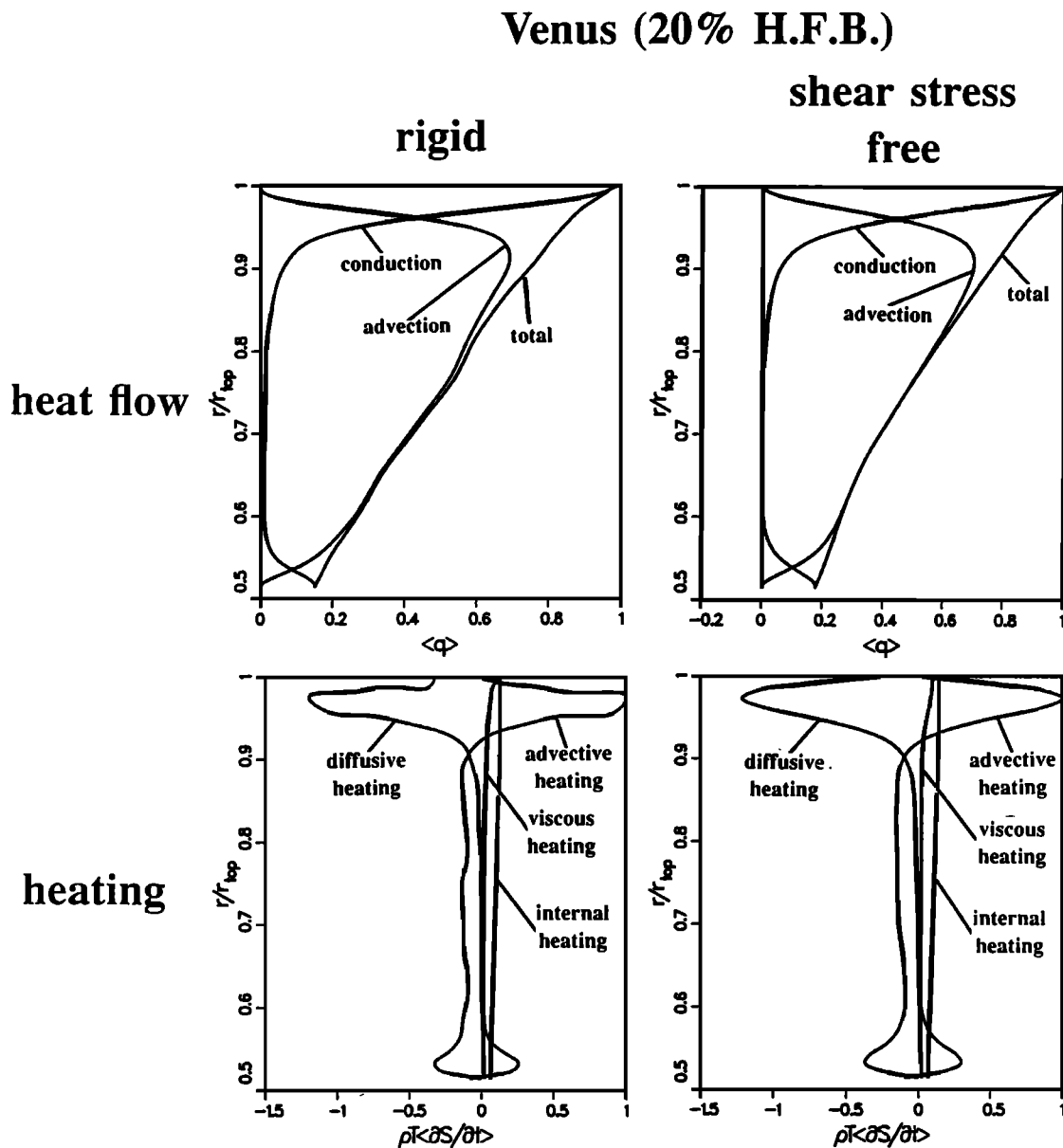


Fig. 17. Similar to Figure 16 but for Venus models in which approximately 20% of the surface heat flow comes from below. The contribution of viscous heating to the energy equation is nonzero for these Venus models.

theory [e.g., Turcotte and Schubert, 1982] and numerical studies [Bercovici et al., 1988], the nondimensional topography $\delta r/(\alpha \Delta T d)$ (where α is a typical thermal expansivity and ΔT is a characteristic temperature scale) is proportional to Ra^f , where f is a number less than 1 ($f=2/3$ in purely basally heated convection and $1/2$ in purely internally heated convection). We can therefore expect more reasonable topographies from Venus models with more realistic viscosities and Rayleigh numbers.

Because Mars has a much thinner mantle than Venus, the Mars models use a more realistic mantle viscosity. Thus the topography calculated for the Mars models is more relevant to actual Mars topography. The models of present Mars with a large core yield peak-to-trough topographic amplitudes of no more than 4 km. However, the small core Mars model yields a peak-to-trough amplitude close to 10 km,

since the extensive buoyant columns of the two plumes provide considerable uplift.

DISCUSSION

Mars

The results presented above for convection in models of the mantles of Mars and Venus show that the cylindrical plume is the prominent form of upwelling as long as sufficient heat enters the mantle from the core. If the proportion of heating from the core is much smaller than the proportion of internal heating, penetrative convection can occur wherein upwelling plumes are eliminated altogether [Machetel and Yuen, 1989]. We can therefore expect major volcanic provinces on Mars, like Tharsis and Elysium,

Mars (90% H.F.B.)

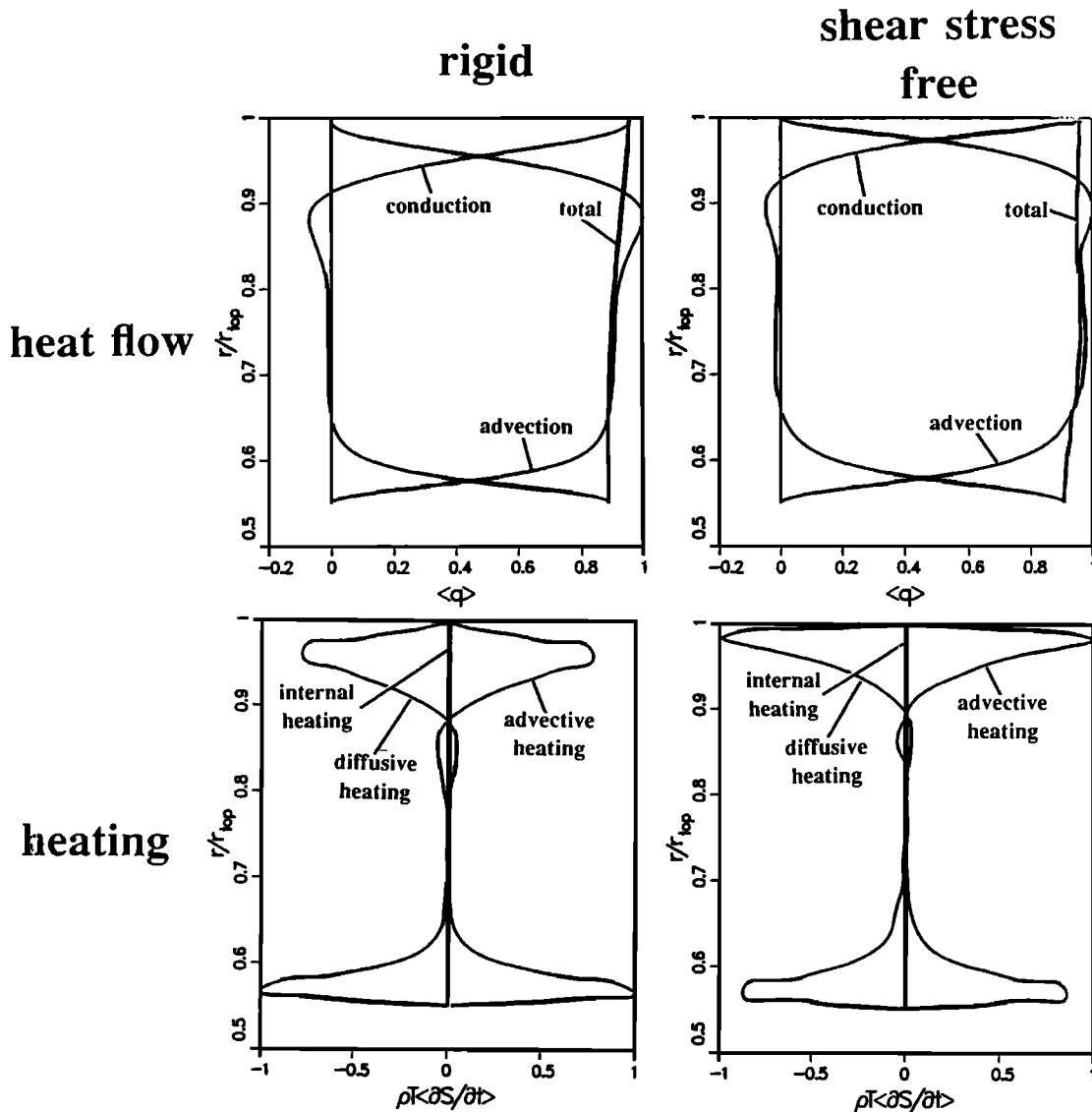


Fig. 18. Similar to Figure 16 but for Mars models that are mainly (approximately 90%) heated from below. Internal heating is very close to zero.

to reflect the cylindrical nature of upwelling mantle plumes, similar to hotspots on Earth. There are no sheet-like upwelling features in the Martian mantle to produce a pattern similar to the linear global system of mid-ocean ridges on the Earth. Even the mid-ocean ridges on Earth are not connected to deep sheet-like upwellings in the Earth's mantle [Bercovici *et al.*, 1989b]. The deep upwellings in models of convection in the Earth's mantle are also cylindrical plumes. The Earth's mid-ocean ridges are shallow, passive upwellings occurring in response to the tearing of lithospheric plates by the pull of descending slabs [Lachenbruch, 1976; Silver *et al.*, 1988; Bercovici *et al.*, 1989b]. When internal heating is predominant, plate tectonics is enhanced by a stress-free top boundary since downwelling sheets are long and temporally durable. Therefore the free motion of the plates on the Earth's surface facilitates the convective circulation that drives the plates. (Although non-Newtonian

rheology of the Earth's lithosphere is essential for the occurrence of plate tectonics, the durability of convective downwelling assists in maintaining the plate motions.) In contrast, a rigid boundary promotes the evanescence of linear systems of slabs, thereby inhibiting even the initiation of slab-driven tectonics. Since Mars is a one-plate planet with a thick lithosphere [Solomon, 1978; Schubert *et al.*, 1979], its downwellings will be short-lived and ineffective in disrupting the lithosphere. Thus the major tectonic features will be hotspots and volcanic domes arising from mantle upwellings in the form of cylindrical plumes. A rigid upper boundary produces nonaxisymmetric variations in the upper thermal boundary layer surrounding hotspots, i.e., downwellings emanating radially from plume axes. These downwellings exert extensional stresses on the lithosphere that might explain the radial fractures on the Tharsis rise.

The results of the spherical convection models have im-

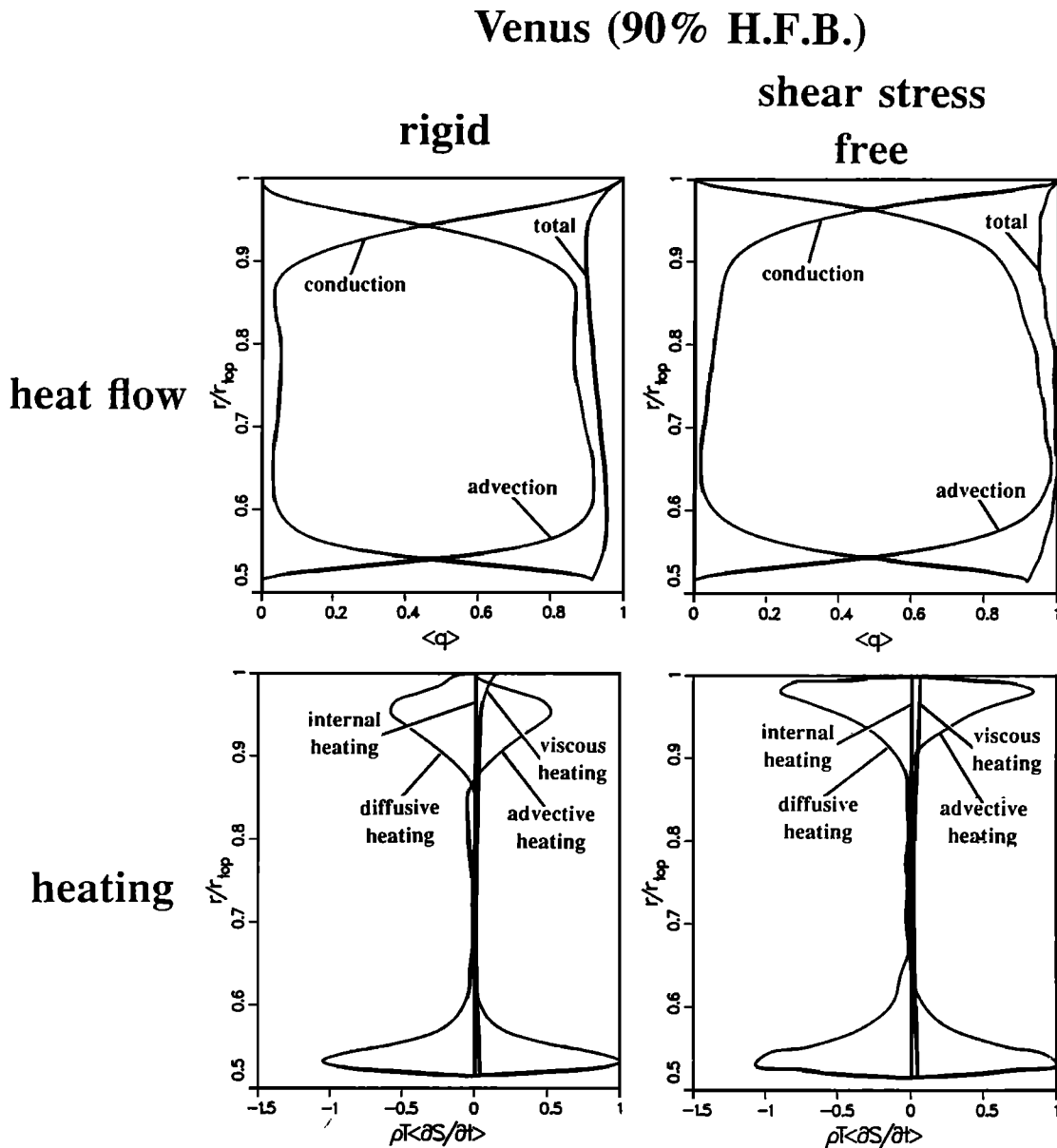


Fig. 19. Similar to Figure 17 but for Venus models that are mainly (approximately 90%) heated from below.

plications for proposed explanations of the Martian crustal dichotomy and the concentrations of volcanism at Tharsis and Elysium. If the crustal dichotomy was caused by a convective system dominated by spherical harmonic degree $\ell = 1$ [Schubert and Lingenfelter, 1973; Lingenfelter and Schubert, 1973; Wise et al., 1979] with upwelling under the northern hemisphere, then the convection was possibly driven strongly from below (while our models produced 6–12 plumes, the number of plumes decreases with increasing percentage of bottom heating). Such strong heating concentrated deep within Mars might arise from the heating pulse accompanying core formation or from the flow of heat from a hot core. Indeed, the overturning accompanying core formation could in itself be an $\ell = 1$ mode [Stevenson, 1980], obviating the need for a thermally driven motion.

During the early stages of core formation, the effective core radius would have been smaller than the radius at

present, favoring a thermally forced convection with perhaps just one dominant upwelling. Since the Martian core formed contemporaneously with accretion or within a few hundred million years of the end of accretion [Chen and Wasserburg, 1986; Schubert et al., 1990], conditions favoring $\ell = 1$ convection, i.e., a small core and a deep heat source, occur very early in the evolution of Mars. If a convective mechanism is responsible for the crustal dichotomy, then the dichotomy is likely a very ancient feature. However, the model in this study for a Mars with a small core consistently produces a convective pattern with a dominant $\ell = 2$ signature; a yet smaller core may be necessary to yield the $\ell = 1$ pattern. Although the $\ell = 2$ planform does not correlate with the crustal dichotomy, it does agree with the geoid signature of Tharsis, which has a strong $\ell = 2$, $m = 2$ component [Kaula, 1979; Christensen and Balmino, 1979; Balmino et al., 1982], where m is the azimuthal order of

Mars (90% H.F.B)

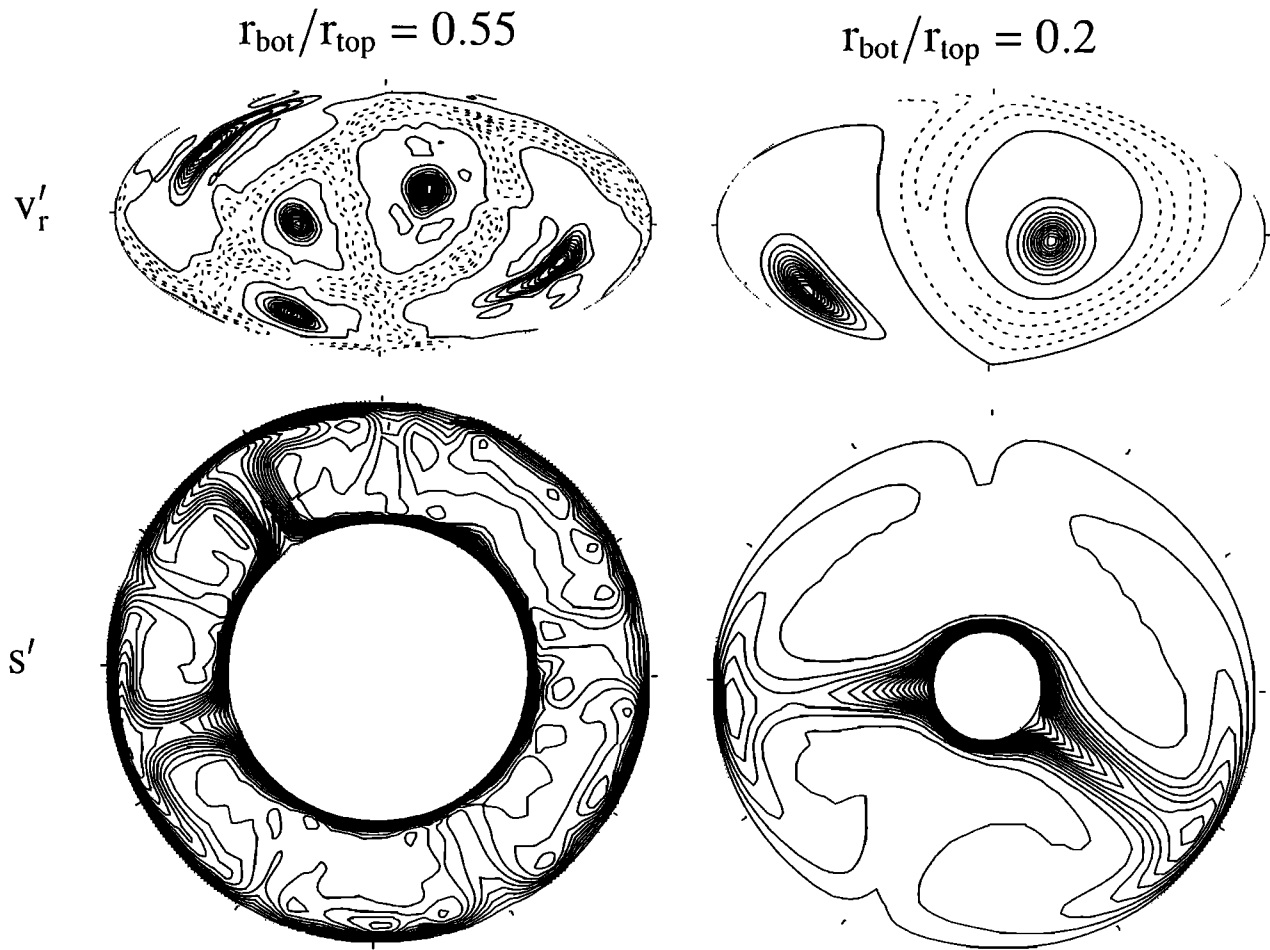


Fig. 20. Comparison of middepth velocity contours and meridional temperature contours for two Mars models with inner-to-outer radius ratios of 0.55 and 0.2. The small core model may be relevant to the early stages of Martian evolution while the core was still forming. The outer surface is rigid in these models, and the shell is mostly (approximately 90%) heated from below.

the spherical harmonic mode. Furthermore, the topography generated by convective stresses in the small core case is in close agreement with that of the Tharsis rise (although the model topography is only an upper limit). Thus the Tharsis rise could have achieved its full height by dynamic uplift in the early evolution of Mars.

The model's dynamic uplift with a present core accounts for 4 of the 10 km of topography in the Tharsis region. The 4 km of dynamic uplift represents uncompensated topography comparable to estimates [Willemann and Turcotte, 1981] of the amount of uncompensated topography associated with the Tharsis rise. It may therefore be unnecessary to invoke elastic support of the uncompensated Tharsis topography. The additional, compensated Tharsis topography is probably largely the result of other processes, such as volcanic construction, magmatic thickening of the crust, or depletion of the underlying mantle [e.g., Sleep and Phillips, 1979, 1985; Solomon and Head, 1982]. It is likely that the Tharsis rise and its volcanic constructs are a consequence of a strong mantle plume (or grouping of plumes) beneath the region.

It is not obvious from the models for a present Mars why there should be only two major volcanic centers [Tharsis and Elysium] on Mars. The models predict several to about 10 major mantle plumes. Perhaps the models are not realistic enough to predict the actual number of major hotspots on Mars. On the other hand, there may be many plumes in the Martian mantle, but the properties of the lithosphere may select only one or two of them for prominent surface expression. Plume activity could be focussed beneath Tharsis if fracturing or thinning of the lithosphere in this region has facilitated magma and heat transport across the lithosphere. The interaction between three-dimensional mantle convection and lithospheric erosion and thinning is an important topic for future research.

Venus

A number of features on the surface of Venus may be associated with cylindrical upwelling plumes in the planet's mantle. The equatorial highlands are quasi-circular features

Mars (90% H.F.B)

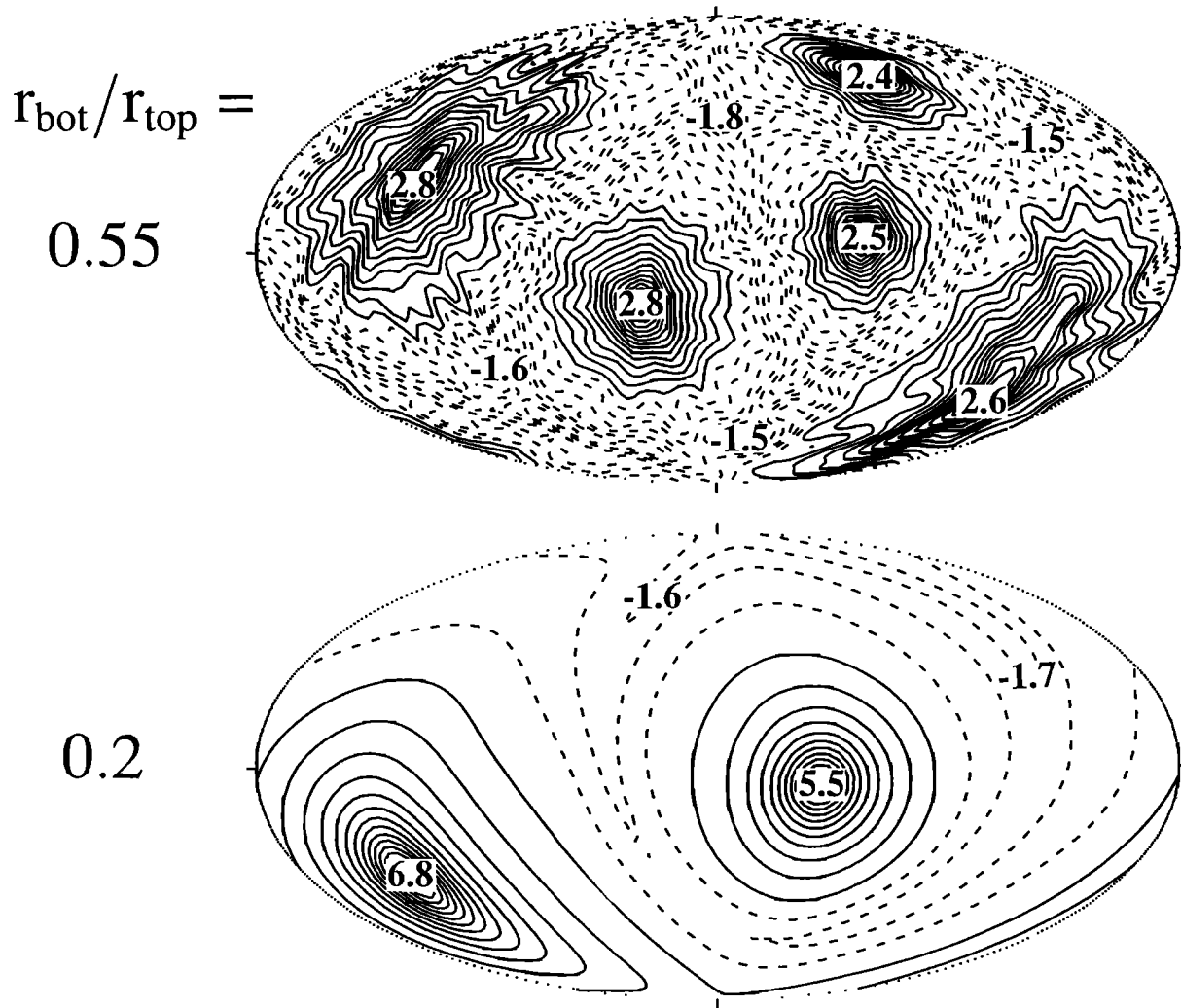


Fig. 21. Surface topography (in km) for the cases of Figure 20. The extrema are labelled to show the maximum and minimum relief.

with prominent geoid anomalies that have been interpreted as surface swells over hot upwelling mantle plumes [Kiefer and Hager, 1988]. Coronae are ovoidal features, 150–600 km in diameter, with encircling ridges and grooves, uplifted by several hundred meters (up to a kilometer) above surrounding terrain, and characterized by interior lava flows and domes indicative of volcanic activity [Barsukov *et al.*, 1986]. It has been suggested that the Venus coronae are also the surface expressions of upwelling mantle plumes [Stofan *et al.*, 1987, 1988; Schubert *et al.*, 1989a; Stofan and Head, 1989].

The large number of coronae and their widespread distribution [Barsukov *et al.*, 1986; Schubert *et al.*, 1989a] argue for the existence of at least several tens of plumes in Venus's mantle, evidence that Venus's mantle like Earth's mantle, is mainly heated from within. Since mantle plumes arise from a thermal boundary layer at the lower boundary of the mantle, the existence of plumes in the mantle of Venus is indirect evidence that the planet has a core. The distribution

of coronae and plume-associated highlands map the anomalously hot regions on Venus's core-mantle boundary. The clustering of coronae at particular locations on Venus could indicate that broad, anomalously hot regions of the core-mantle boundary give rise to multiple plumes, as may also be occurring at Earth's core-mantle boundary, for example, beneath the Pacific [Dziewonski and Woodhouse, 1987; Silver *et al.*, 1988]. Alternatively, the clustering of plumes and their surface expressions as coronae could be a consequence of thinned or fractured lithosphere focussing plume activity to particular sites, as may also be the case beneath Tharsis.

The diameters of coronae are smaller than the plume diameters in our constant viscosity Venus models. The incorporation of more realistic temperature-dependent viscosity into the models would result in much narrower plumes [Olson *et al.*, 1988; Schubert *et al.*, 1989b, 1990]. The heights of coronae are also much smaller than the model predictions of dynamic topography above plumes. This can also be attributed to lack of a sufficiently realistic viscosity in

the models and to a model Rayleigh number that is smaller than the actual Rayleigh number in Venus's mantle.

It is possible that there is a limited amount of crustal spreading from linear features in Aphrodite, similar to seafloor spreading from mid-ocean ridges on Earth [Head and Crumpler, 1987; Crumpler and Head, 1988, 1989]. If Aphrodite has been formed by several closely spaced mantle plumes, then the apparent ridgelike features in Aphrodite could result from shallow linear upwellings that connect the plumes. Alternatively, the rheology of Venus's lithosphere in the Aphrodite region may have terrestrial plate-like characteristics that cause it to tear or pull apart along linear features that become shallow, passive, secondary centers of upwelling. The models of spherical convection in Venus's mantle presented in this paper have no deep-seated, active, linear upwellings that could be associated with linear spreading centers in Aphrodite.

Acknowledgments. This work has benefitted from the Los Alamos National Laboratory Mantle Convection Workshop, sponsored by the Institute for Geophysics and Planetary Physics. This work was supported by grant NAG5152 from NASA and a computing grant from the San Diego Supercomputer Center.

REFERENCES

- Balmino, G., B. Moynot, and N. Vales, Gravity field model of Mars in spherical harmonics, *J. Geophys. Res.*, **87**, 9735-9746, 1982.
- Barsukov, V. L., et al., The geology and geomorphology of the Venus surface as revealed by the radar images obtained by Veneras 15 and 16, *Proc. Lunar Planet. Sci. Conf. 16th*, Part 2, *J. Geophys. Res.*, **91**, Suppl., D378-D398, 1986.
- Baumgardner, J. R., Application of supercomputers to 3-d mantle convection, in *The Physics of the Planets* edited by S.K. Runcorn, pp. 199-231, John Wiley, New York, 1988.
- Bercovici, D., G. Schubert, and A. Zebib, Geoid and topography for infinite Prandtl number convection in a spherical shell, *J. Geophys. Res.*, **93**, 6430-6436, 1988.
- Bercovici, D., G. Schubert, G. A. Glatzmaier, and A. Zebib, Three-dimensional thermal convection in a spherical shell, *J. Fluid Mech.*, **206**, 75-104, 1989a.
- Bercovici, D., G. Schubert, and G. A. Glatzmaier, Three-dimensional, spherical models of convection in the Earth's mantle, *Science*, **244**, 950-955, 1989b.
- Bercovici, D., G. Schubert, and G. A. Glatzmaier, Influence of heating mode on three-dimensional mantle convection, *Geophys. Res. Lett.*, **16**, 617-620, 1989c.
- Chandrasekhar, S., *Hydrodynamic and Hydromagnetic Stability*, Oxford University Press, New York, 1961.
- Chen, J. H., and G. J. Wasserburg, Formation ages and evolution of shergotty and its parent from U-Th-Pb systematics, *Geochim. Cosmochim. Acta*, **50**, 955-968, 1986.
- Christensen, E. J., and G. Balmino, Development and analysis of a twelfth degree and order gravity model for Mars, *J. Geophys. Res.*, **84**, 7943-7953, 1979.
- Crumpler, L. S., and J. W. Head, Bilateral topographic symmetry patterns across Aphrodite Terra, Venus, *J. Geophys. Res.*, **93**, 301-312, 1988.
- Crumpler, L. S., and J. W. Head, Eastern Aphrodite Terra, Venus: Evidence for additional divergent plate-boundary characteristics and crustal spreading from Diana Chasma to Atla Regio, *Lunar Planet. Sci.*, **XX**, 214-215, 1989.
- Dziewonski, A. M., and J. H. Woodhouse, Global images of the Earth's interior, *Science*, **236**, 37-48, 1987.
- Glatzmaier, G. A., Numerical simulations of stellar convective dynamos, I, The model and method, *J. Comput. Phys.*, **55**, 461-484, 1984.
- Glatzmaier, G. A., Numerical simulations of mantle convection: time-dependent, three-dimensional, compressible, spherical shell, *Geophys. Astrophys. Fluid Dyn.*, **43**, 223-264, 1988.
- Head, J. W., III, and L. S. Crumpler, Evidence for divergent plate-boundary characteristics and crustal spreading on Venus, *Science*, **238**, 1380-1385, 1987.
- Kaula, W. M., The moment of inertia of Mars, *Geophys. Res. Lett.*, **6**, 194-196, 1979.
- Kaula, W. M., and R. J. Phillips, Quantitative tests for plate tectonics on Venus, *Geophys. Res. Lett.*, **8**, 1187-1190, 1981.
- Kiefer, W. S., and B. H. Hager, Mantle plumes on Venus: A model for the equatorial highlands and a possible connection with the ovoids, *Lunar Planet. Sci.*, **XLX**, 601-602, 1988.
- Lachenbruch, A. H., Dynamics of a passive spreading center, *J. Geophys. Res.*, **81**, 1883-1902, 1976.
- Lingenfelter, R. E., and G. Schubert, Evidence for convection in planetary interiors from first-order topography, *Moon*, **7**, 172-180, 1973.
- Machetel, P., and D. A. Yuen, Penetrative convective flows induced by internal heating and mantle compressibility, *J. Geophys. Res.*, **94**, 10,609-10,626, 1989.
- Olson, P., G. Schubert, C. Anderson, and P. Goldman, Plume formation and lithosphere erosion: A comparison of laboratory and numerical experiments, *J. Geophys. Res.*, **93**, 15,065-15,084, 1988.
- Phillips, R. J., W. M. Kaula, G. E. McGill, and M. C. Malin, Tectonics and evolution of Venus, *Science*, **212**, 879-887, 1981.
- Schubert, G., Subsolidus convection in the mantles of terrestrial planets, *Annu. Rev. Earth Planet. Sci.*, **7**, 289-342, 1979.
- Schubert, G., and R. E. Lingenfelter, Martian center of mass-center of figure offset, *Nature*, **242**, 251-252, 1973.
- Schubert, G., and T. Spohn, Thermal history of Mars and the sulfur content of its core, *J. Geophys. Res.* this issue.
- Schubert, G., P. Cassen, and R. E. Young, Subsolidus convective cooling histories of terrestrial planets, *Icarus*, **38**, 192-211, 1979.
- Schubert, G., D. Bercovici, P. J. Thomas and D. B. Campbell, Venus coronae: Formation by mantle plumes, *Lunar Planet. Sci.*, **XX**, 968-969, 1989 a.
- Schubert, G., P. Olson, C. Anderson, and P. Goldman, Solitary waves in mantle plumes, *J. Geophys. Res.*, **94**, 9523-9532, 1989b.
- Schubert, G., S. C. Solomon, D. L. Turcotte, M. J. Drake, and N. H. Sleep, Origin and thermal evolution of Mars, in *Mars*, edited by H. Kieffer, B. Jakosky, C. Snyder, and M. S. Matthews, University of Arizona Press, Tucson, in press, 1990.
- Silver, P. G., R. W. Carlson, and P. Olson, Deep slabs, geochemical heterogeneity, and the large-scale structure of mantle convection: Investigation of an enduring paradox, *Annu. Rev. Earth Planet. Sci.*, **16**, 477-541, 1988.
- Sleep, N. H., and R. J. Phillips, An isostatic model for the Tharsis province, Mars, *Geophys. Res. Lett.*, **6**, 803-806, 1979.
- Sleep, N. H., and R. J. Phillips, Gravity and lithospheric stress on the terrestrial planets with reference to the Tharsis region of Mars, *J. Geophys. Res.*, **90**, 4469-4489, 1985.
- Solomon, S. C., On volcanism and thermal tectonics on one-plate planets, *Geophys. Res. Lett.*, **5**, 461-464, 1978.
- Solomon, S. C., and J. W. Head, Evolution of the Tharsis province of Mars: The importance of heterogeneous lithospheric thickness and volcanic construction, *J. Geophys. Res.*, **87**, 9755-9774, 1982.
- Stevenson, D. J., Lunar symmetry and paleomagnetism, *Nature*, **287**, 520-521, 1980.
- Stevenson, D. J., T. Spohn, and G. Schubert, Magnetism and thermal evolution of the terrestrial planets, *Icarus*, **54**, 466-489, 1983.
- Stofan, E. R., and J. W. Head, Coronae of Mnemosyne Region, Venus: Morphology and origin, *Lunar Planet. Sci.*, **XX**, 1061-1062, 1989.
- Stofan, E. R., J. W. Head, and E. M. Parmentier, Corona structures on Venus: Models of origin, *Lunar Planet. Sci.*, **XVIII**, 954-955, 1987.
- Stofan, E. R., J. W. Head, and E. M. Parmentier, Corona structures on Venus: Evidence for a diapiric origin, *Lunar Planet. Sci.*, **XIX**, 1129-1130, 1988.
- Turcotte, D. L., and G. Schubert, *Geodynamics*, 450 pp., John Wiley, New York, 1982.

- Willemann, R. J., and D. L. Turcotte, Support of topographic and other loads on the Moon and on the terrestrial planets, *Proc. Lunar Planet. Sci.*, 12B, 837-851, 1981.
- Wise, D. U., M. P. Golombek, and G. E. McGill, Tectonic evolution of Mars, *J. Geophys. Res.*, 84, 7934-7939, 1979.
- Zebib, A., G. Schubert, J. L. Dein, and R. C. Paliwal, Character and stability of axisymmetric thermal convection in spheres and spherical shells, *Geophys. Astrophys. Fluid Dyn.*, 23, 1-42, 1983.

D. Bercovici, Department of Geology and Geophysics, Woods Hole Oceanographic Institution, Woods Hole, MA 02543.

G. A. Glatzmaier, ESS-5 MS-F665, Los Alamos National Laboratory, Los Alamos, NM 87545

G. Schubert, Department of Earth and Space Sciences, University of California, Los Angeles, CA 90024-1567

(Received July 17, 1989;
revised March 27, 1990;
accepted April 9, 1990)